

**Louisiana Water Resources Research Institute
Annual Technical Report
FY 2012**

Introduction

This report presents a description of the activities of the Louisiana Water Resources Research Institute for the period of March 1, 2012 to February 28, 2013 under the direction of Dr. John Pardue. The Louisiana Water Resources Research Institute (LWRRI) is unique among academic research institutions in the state because it is federally mandated to perform a statewide function of promoting research, education and services in water resources. The federal mandate recognizes the ubiquitous involvement of water in environmental and societal issues, and the need for a focal point for coordination.

As a member of the National Institutes of Water Resources, LWRRI is one of a network of 54 institutes nationwide initially authorized by Congress in 1964 and has been re-authorized through the Water Resources Research Act of 1984, as amended in 1996 by P.L. 104-147. Under the Act, the institutes are to:

"1) plan, conduct, or otherwise arrange for competent research that fosters, (A) the entry of new research scientists into water resources fields, (B) the training and education of future water scientists, engineers, and technicians, (C) the preliminary exploration of new ideas that address water problems or expand understanding of water and water-related phenomena, and (D) the dissemination of research results to water managers and the public.

2) cooperate closely with other colleges and universities in the State that have demonstrated capabilities for research, information dissemination and graduate training in order to develop a statewide program designed to resolve State and regional water and related land problems. Each institute shall also cooperate closely with other institutes and organizations in the region to increase the effectiveness of the institutes and for the purpose of promoting regional coordination."

The National Water Resources Institutes program establishes a broad mandate to pursue a comprehensive approach to water resource issues that are related to state and regional needs. Louisiana is the water state; no other state has so much of its cultural and economic life involved with water resource issues. The oil and gas industry, the chemical industry, port activities, tourism and fisheries are all dependent upon the existence of a deltaic landscape containing major rivers, extensive wetlands, numerous large shallow water bays, and large thick sequences of river sediments all adjacent to the Gulf of Mexico.

History of the Institute

Louisiana has an abundance of water resources, and while reaping their benefits, also faces complex and crucial water problems. Louisiana's present water resources must be effectively managed, and the quality of these resources must be responsibly protected. A fundamental necessity is to assure continued availability and usability of the state's water supply for future generations. Specifically, Louisiana faces five major issues that threaten the quality of the state's water supply, which are also subsets of the southeastern/island region priorities:

Nonpoint sources of pollution are estimated to account for approximately one-half of Louisiana's pollution. Because of the potential impact of this pollution and the need to mitigate its effects while maintaining the state's extensive agricultural base and coastal zones, continued research is needed in the area of nonpoint issues. Louisiana's regulatory agencies are addressing non-point source problems through the development of waste load allocation models or total maximum daily load (TMDL) calculations. There are serious technical issues that still require resolution to insure that progress is made in solving the non-point source problem.

Louisiana's vast wetlands make up approximately 40% of the nation's wetlands. These areas are composed of very sensitive and often delicately balanced ecosystems which make them particularly vulnerable to

contamination or destruction resulting both from human activities and from natural occurrences. Understanding these threats and finding management alternatives for the state's unique wetland resources are priority issues needing attention.

Water resources planning and management are ever-present dilemmas for Louisiana. Severe flooding of urban and residential areas periodically causes economic loss and human suffering, yet solutions to flooding problems can be problems in themselves. Water supply issues have also recently a focus of concern. Despite the abundance of resources, several aquifers have been in perennial overdraft, including the Chicot aquifer. Louisiana passed its first legislation that restricts groundwater use in the past year. Water resources and environmental issues are intricately interconnected; therefore, changes in one aspect produce a corresponding responsive change in another. Further study is needed to understand these relationships.

Water quality protection, particularly of ground water resources, is an area of concern in Louisiana. Researchers are beginning to see contamination in drinking water supplies that was not present in the past. Delineating aquifer recharge areas, understanding the impacts of industrial activities on water resources, evaluating nonpoint sources of pollution, and exploring protection alternatives are issues at the forefront.

Wastewater management has been a long-standing issue in Louisiana. The problem of wastewater management focuses primarily on rural and agricultural wastewater and the high costs for conventional types of wastewater treatment as found in the petrochemical industry.

The Institute is administratively housed in the College of Engineering and maintains working relationships with several research and teaching units at Louisiana State University. Recent cooperative research projects have been conducted with the University of New Orleans and the EPA's Hazardous Substance Research Center- South & Southwest.

LWRRRI and the Deepwater Horizon Oil Spill

During this reporting period, LWRRRI continued its work on the Deepwater Horizon oil spill. The LWRRRI director advised state and national agencies, conducted ongoing research on the fate of oil in the systems and organized and presented research results at local, regional and national meetings. Details of this activity are presented below in the "Notable Achievements" section of the report.

Research Program Introduction

The primary goal of the Institute is to help prepare water professionals and policy makers in the State of Louisiana to meet present and future needs for reliable information concerning national, regional, and state water resources issues. The specific objectives of the Institute are to fund the development of critical water resources technology, to foster the training of students to be water resources scientists and engineers capable of solving present and future water resources problems, to disseminate research results and findings to the general public, and to provide technical assistance to governmental and industrial personnel and the citizens of Louisiana.

The priority research areas for the Institute in FY 2012 focused on selected research themes developed in conjunction with the advisory board. These themes corresponded to the major water resource areas affecting Louisiana described in the Introduction above. Projects selected were from a range of faculty with different academic backgrounds including geological scientists, environmental engineers and water resource engineers and scientists. Supporting research in these priority areas has increased the visibility of the Institute within the State.

The individual research projects designated as Projects 2012LAXXXX, are listed below.

- Project 2010LA76G, Tsai & Hanor - Hierarchical Multimodel Saltwater Intrusion Remediation and Sampling Designs: A BMA Tree Approach
- Project 2012LA83B- White and Bargu, Nutrient and harmful algal bloom (HAB) dynamics in Lake Pontchartrain during a non-spillway opening year
- Project 2012LA84B - Deng, Identification of Contaminant Source Locations in Amite River Watershed • Project 2012LA85B- Tsai, Hydrostratigraphy Modeling of the Southern Hills Aquifer System and Faults
- Project 2012LA87B--Smith, Irregular Wave Dissipation by Coastal Vegetation

These projects include one project that focus on climate and hydrologic processes (Project 2012LA87B), two projects that focus on groundwater flow and transport (Projects 2010LA76G and 2012LA85B), one project that focuses on Biological Sciences (2012LA83B) and one project that focuses on watershed research (Project 2012LA84B)

Hierarchical Multimodel Saltwater Intrusion Remediation and Sampling Designs: A BMA Tree Approach

Basic Information

Title:	Hierarchical Multimodel Saltwater Intrusion Remediation and Sampling Designs: A BMA Tree Approach
Project Number:	2010LA76G
Start Date:	9/1/2010
End Date:	8/31/2013
Funding Source:	104G
Congressional District:	Louisiana
Research Category:	Ground-water Flow and Transport
Focus Category:	Groundwater, Management and Planning, Methods
Descriptors:	
Principal Investigators:	Frank Tsai, Jeff Hanor

Publications

1. Tsai, F.T.-C. (2011). Scavenger Wells Stop Saltwater Intrusion in Baton Rouge, Louisiana, IGWMC MODFLOW and More 2011 Conference: Integrated Hydrologic Modeling, Golden, Colorado, June 5-8, 2011.
2. Tsai, F. T.-C., and Ahmed S. Elshall (2011). A Hierarchical Bayesian Model Averaging Approach to Cope With Sources of Uncertainty in Conceptual Ground Water Models, World Water & Environmental Resources Congress, Palm Springs, California, May 22-26, 2011.
3. Tsai, F. T.-C. (2011). Stop Saltwater Intrusion Toward Water Wells Using Scavenger Wells, World Water & Environmental Resources Congress, Palm Springs, California, May 22-26, 2011.
4. Callie E. Anderson and Jeffrey S. Hanor (2011) Origin of waters causing salinization of the Baton Rouge aquifer system, Louisiana. South-Central Section Geological Society of America 45th Annual Meeting, March 27-29, 2011.
5. Frank T.-C. Tsai (2011). Saltwater Intrusion Simulation in the “1,500-Foot” Sand of the Baton Rouge Area: Pre-Anthropogenic Pumping, Current Situation, Future, Fifth Annual Louisiana Groundwater, Coastal Geology and Subsidence-Land Loss Symposia, Baton Rouge, Louisiana, January 11-12, 2011.
6. Callie E. Anderson and Jeffrey S. Hanor (2011) The St. Gabriel salt dome as a potential source of the salty waters contaminating the Baton Rouge aquifer system. Fifth Annual Louisiana Groundwater, Coastal Geology and Subsidence-Land Loss Symposia, Baton Rouge, Louisiana, January 11-12, 2011.
7. Ahmed Elshall and Frank T.-C. Tsai (2011). Geophysical and geostatistical approaches to subsurface characterization of the Baton Rouge area, Fifth Annual Louisiana Groundwater, Coastal Geology and Subsidence-Land Loss Symposia, Baton Rouge, Louisiana, January 11-12, 2011.
8. Nima Chitsazan and Frank T.-C. Tsai (2011). Bed boundary delineation of “1,500-foot”, “1,700-foot”, and “2,000-foot sands of the Baton Rouge area, Fifth Annual Louisiana Groundwater, Coastal Geology and Subsidence-Land Loss Symposia, Baton Rouge, Louisiana, January 11-12, 2011.
9. Tsai, F. T.-C. (2010). “1,500-Foot” Sand Saltwater Intrusion Simulation and Management Using Scavenger Wells, Baton Rouge Geological Society, Baton Rouge, Louisiana, December 10, 2010. (invited)

Hierarchical Multimodel Saltwater Intrusion Remediation and Sampling Designs: A BMA Tree Approach

10. Tsai, F.T.-C. (2010), Scavenger Wells Stop Saltwater Intrusion in Baton Rouge, 2010 Louisianan Water Quality Technology Conference, Alexandria and Baton Rouge, Louisiana, December 14-15, 2010. (invited)
11. Tsai, F.T.-C. (2010) Scavenger Well Operation to Stop Saltwater Intrusion Toward BRWC Lula Wells in the Baton Rouge Area, Louisiana Capital Area Ground Water Conservation Commission, September 14, 2010. (invited)
12. • Frank Tsai, 2012, Feasibility Study of Scavenging Approach to Stop Saltwater Toward Water Wells, Louisiana State University, Baton Rouge, Louisiana, 10 pages. (USGS 104B)
13. Tsai, F. T.-C., and A.S. Elshall. (2011). A Hierarchical Bayesian Model Averaging Approach to Cope With Sources of Uncertainty in Conceptual Ground Water Models, World Water & Environmental Resources Congress, Palm Springs, CA, May 22-26, 2011.
14. Tsai, F. T.-C. (2011). Development of Scavenger Well Operation Model To Stop Saltwater Intrusion Toward Water Wells In The “1,500-Foot” Sand of The Baton Rouge Area, Louisiana, World Water & Environmental Resources Congress, Palm Springs, CA, May 22-26, 2011.
15. Tsai, F. T.-C. (2011). Scavenger Wells Stop Saltwater Intrusion in Baton Rouge, Louisiana, MODFLOW and More 2011, Golden, CO, June 5-8, 2011
16. • Frank Tsai, 2012, Feasibility Study of Scavenging Approach to Stop Saltwater Toward Water Wells, Louisiana State University, Baton Rouge, Louisiana, 10 pages. (USGS 104B)
17. Tsai, F. T.-C., and A.S. Elshall. (2011). A Hierarchical Bayesian Model Averaging Approach to Cope With Sources of Uncertainty in Conceptual Ground Water Models, World Water & Environmental Resources Congress, Palm Springs, CA, May 22-26, 2011.
18. Tsai, F. T.-C. (2011). Development of Scavenger Well Operation Model To Stop Saltwater Intrusion Toward Water Wells In The “1,500-Foot” Sand of The Baton Rouge Area, Louisiana, World Water & Environmental Resources Congress, Palm Springs, CA, May 22-26, 2011.
19. Tsai, F. T.-C. (2011). Scavenger Wells Stop Saltwater Intrusion in Baton Rouge, Louisiana, MODFLOW and More 2011, Golden, CO, June 5-8, 2011
20. Elshall, A. S., F. T.-C. Tsai, J. S. Hanor, Indicator geostatistics for reconstructing Baton Rouge aquifer-fault hydrostratigraphy (Louisiana, USA), Hydrogeology Journal, 2013. (accepted)
21. Tsai, F. T.-C. and A. S. Elshall, Hierarchical Bayesian model averaging for hydrostratigraphic modeling: Uncertainty segregation and comparative evaluation, Water Resources Research, 2013. (accepted)
22. Nadiri, A.A., N. Chitsazan, F. T.-C. Tsai, and A. Asghari Moghaddam. Bayesian Artificial Intelligence Model Averaging for Hydraulic Conductivity Estimation. ASCE Journal of Hydrologic Engineering, 2013. (accepted)
23. Nadiri, A.A., E. Fijani, F. T.-C. Tsai, and A. Asghari Moghaddam. Supervised Committee Machine with Artificial Intelligence for Prediction of Fluoride Concentration, Journal of Hydroinformatics, 2013. (accepted)
24. Chamberlain, Elizabeth Laurel, Depositional Environments of Upper Miocene through Pleistocene Siliciclastic Sediments, Baton Rouge Aquifer System, Southeastern Louisiana, Master of Science Thesis, Department of Geology and Geophysics, Louisiana State University, 66p.
25. Frank Tsai, 2012, Feasibility Study of Scavenging Approach to Stop Saltwater Toward Water Wells, Louisiana State University, Baton Rouge, Louisiana, 10 pages. (USGS 104B)
26. Frank Tsai, 2013, Hydrostratigraphy Modeling of the Southern Hills Aquifer System and Faults, Louisiana State University, Baton Rouge, Louisiana, 10 pages. (USGS 104B)
27. Tsai F. T.-C. Tsai, and A. S. Elshall, A Bayesian Model Averaging Method to Characterize the Baton Rouge Aquifer System, 2012 World Environmental & Water Resources Congress, Albuquerque, NM, May 20-24, 2012
28. Tsai, F. T.-C., A. Mani, H. V. Pham, E. Beigi, A. S. Elshall, and N. Chitsazan, Characterization of Siliciclastic Aquifer-Fault System for Southeastern Louisiana, 2013 World Environmental & Water Resources Congress, Cincinnati, OH, May 19-23, 2013

29. Pham, H. V., A. S. Elshall, F. T.-C. Tsai, and L. Yan, Parallel Inverse Groundwater Modeling Using CMA-ES, 2013 World Environmental & Water Resources Congress, Cincinnati, OH, May 19-23, 2013
30. Hanor, J. S., E. L. Chamberlain and F. T.-C. Tsai, A Conceptual Model for the Evolution of the Permeability Architecture of the Baton Rouge Fault Zone, Southeastern Louisiana, 7th Annual Groundwater and Water Resources Symposia, Baton Rouge, LA, 8 May 2013.
31. Elshall, A. S., F. T.-C. Tsai and J. S. Hanor, Reconstructing Baton Rouge aquifer-fault hydrostratigraphy using indicator geostatistics, 7th Annual Groundwater and Water Resources Symposia, Baton Rouge, LA, 8 May 2013
32. Pham, H. V. and F. T.-C. Tsai, Development of groundwater model for the “1,200-foot”, “1,500-foot” and “1,700-foot” sands of the Baton Rouge area, Southeastern Louisiana, 7th Annual Groundwater and Water Resources Symposia, Baton Rouge, LA, 8 May 2013.
33. Beigi, E. and F. T.-C. Tsai, Modeling of Potential Groundwater Recharge under Climate Change of Southern Hills Aquifer System, Southeastern Louisiana and Southwestern Mississippi, 7th Annual Groundwater and Water Resources Symposia, Baton Rouge, LA, 8 May 2013
34. Beigi, E., and F. T.-C. Tsai, Climate Impact on Groundwater Recharge in Southeastern Louisiana and Southwestern Mississippi, H13B-1317 Abstract, 2012 American Geophysical Union Fall Meeting, San Francisco, CA, 3-7 December 2012.
35. Elshall, A. S., F. T.-C. Tsai, J. S. Hanor, Hydrogeophysical Data Fusion and Geostatistical Approach to Characterize Hydrogeological Structure of the Baton Rouge Aquifer System in Louisiana, H13B-1336 Abstract, 2012 American Geophysical Union Fall Meeting, San Francisco, CA, 3-7 December 2012.
36. Pham, H. V., A. S. Elshall, F. T.-C. Tsai, and L. Yan, Local Derivative-Free Parallel Computing Method for Solving the Inverse Problem in Groundwater Modeling, H21A-1164 Abstract, 2012 American Geophysical Union Fall Meeting, San Francisco, CA, 3-7 December 2012.
37. Chitsazan, N. and F. T.-C. Tsai, Hierarchical Bayesian Model Averaging for Chance Constrained Remediation Designs, H33I-1450 Abstract, 2012 American Geophysical Union Fall Meeting, San Francisco, CA, 3-7 December 2012
38. Tsai, F. T.-C., A. S. Elshall and J. S. Hanor, A Hierarchical Multi-Model Approach for Uncertainty Segregation, Prioritization and Comparative Evaluation of Competing Modeling Propositions, H43B-1326 Abstract, 2012 American Geophysical Union Fall Meeting, San Francisco, CA, 3-7 December 2012
39. Chamberlain, E. L., J. S. Hanor, and F. T.-C. Tsai, Sequence Stratigraphic Characterization of Upper Miocene through Pleistocene Siliciclastic Aquifer Sediments, Baton Rouge Area, Southeastern Louisiana Gulf Coast, H13B-1325 Abstract, 2012 American Geophysical Union Fall Meeting, San Francisco, CA, 3-7 December 2012
40. Nadiri, A. A., N. Chitsazan, F. T.-C. Tsai, and A. Asghari Moghaddam, Bayesian Model Averaging of Artificial Intelligence Models for Hydraulic Conductivity Estimation, H13B-1338 Abstract, 2012 American Geophysical Union Fall Meeting, San Francisco, CA, 3-7 December 2012
41. Fijani, E., N. Chitsazan, A. A. Nadiri, F. T.-C. Tsai, and A. Asghari Moghaddam, Hierarchical Bayesian Model Averaging for Non-Uniqueness and Uncertainty Analysis of Artificial Neural Networks, H43B-1343 Abstract, 2012 American Geophysical Union Fall Meeting, San Francisco, CA, 3-7 December 2012

Problem and Research Objectives

Water use in Baton Rouge, Louisiana is approximately 171.41 million gallons per day out of which 87.4% is ground water and the rest is surface water (Sargent, 2012). Population served by public supply is 436,650. Due to excessive ground water pumping, saltwater is intruding from the saline aquifers in the south part of the Baton Rouge Fault. Thus, in the absence of any remediation measure, some of public supply water wells in East Baton Rouge Parish are under the threat of being abandoned in the near future. The project objective is to develop saltwater intrusion models to be employed for the management and remediation of the ground water resources for the study area shown in Figure 1. The study area is approximately 500 km².

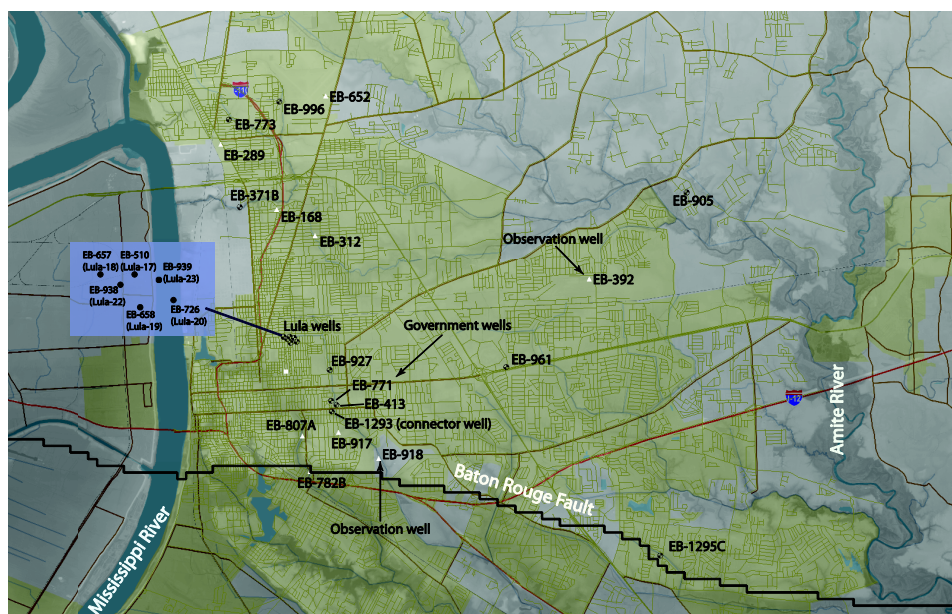


Figure 1: The map of the study area. Circles are pumping wells. White triangles are USGS water wells. All wells in the map were screened at the “1,500-foot” sand.

Due to limited amount of data and since model uncertainty always exists, multiple models are usually developed. Model selection, model elimination, model reduction, and model discrimination are commonly used to select the best model. It is clear that modeling uncertainty is always underestimated if only the best model is used. One would ask why only the best model is used afterwards when so many efforts have been devoted to calibrating many models. This certainly wastes valuable resources and important information from other good models. Hierarchical Bayesian model averaging (HBMA) (Chitsazan and Tsai, 2012; Tsai and Elshall, 2013) best utilize all possible models for model prediction and application under Bayesian statistical framework. HBMA presents several advantages over model selection: (1) Information from all possible models is used based on their model importance (model weights). Calibration efforts are not wasted. (2) The model importance is based on the evidence of data, which avoids over-confidence in the best model that does not have a dominant model weight. And (3) model structure uncertainty is increased and is better presented than that by using a single model. Moreover, HBMA is able to distinguish model uncertainty arising from individual models and

between models. HBMA is able to identify unfavorable models even though they may present small prediction uncertainty.

In this study, the HBMA is used to predict chloride concentration and estimate prediction uncertainty for the “1,500-foot” sand in the Baton Rouge aquifer system. The HBMA is applied to analyze the conceptual model structure uncertainty arising from the different competing model propositions for chloride concentration predictions at the USGS water quality wells.

Methodology

Hierarchical Bayesian Model Averaging (HBMA)

To cope with different sources of uncertainty in groundwater flow and mass transport models, a hierarchical Bayesian model averaging is developed (Tsai and Elshall, 2013). Consider $M_{\underbrace{(ij\dots lm)}_p} \in \mathbf{M}_p$ a model at level p . The subscript $\underbrace{(ij\dots lm)}_p$ locates the model

hierarchically top down from the first level, to the second level and so forth to reach to level p . For example, $M_{(i)} \in \mathbf{M}_1$ is model i at level 1, $M_{(ij)} \in \mathbf{M}_2$ is model j at level 2, which is a child model to parent model i at level 1. $M_{(ijk)} \in \mathbf{M}_3$ is model k at level 3, which is a child model to the parent model j at level 2 and the grandparent model of model i at level 1. From bottom up, parent models \mathbf{M}_{p-1} at level $p-1$ is composed of the child models \mathbf{M}_p at level p . Models \mathbf{M}_{p-2} at level $p-2$ are composed of models \mathbf{M}_{p-1} at level $p-1$ and so forth until the Hierarch BMA model M_0 is reached.

Consider base models at level p . According to the law of total probability, the posterior probability for predicted quantity Δ given data \mathbf{D} is

$$\Pr(\Delta | \mathbf{D}) = E_{\mathbf{M}_1} E_{\mathbf{M}_2} \dots E_{\mathbf{M}_p} \left[\Pr(\Delta | \mathbf{D}, \mathbf{M}_p) \right], \quad (1)$$

where $E_{\mathbf{M}_p}$ is the expectation operator with respect to models \mathbf{M}_p at level p . $\Pr(\Delta | \mathbf{D}, \mathbf{M}_p)$ is the posterior probability of predicted quantity Δ given data \mathbf{D} and models \mathbf{M}_p at level p . The expectation $E_{\mathbf{M}_p} [\Pr(\Delta | \mathbf{D}, \mathbf{M}_p)]$ is posterior probability averaging at level p . That is

$$E_{\mathbf{M}_p} \left[\Pr(\Delta | \mathbf{D}, \mathbf{M}_p) \right] = \sum_m \Pr \left(\Delta | \mathbf{D}, M_{\underbrace{(ij\dots lm)}_p} \right) \Pr \left(M_{\underbrace{(ij\dots lm)}_p} | \mathbf{D}, M_{\underbrace{(ij\dots l)}_{p-1}} \right). \quad (2)$$

where $\Pr \left(\Delta | \mathbf{D}, M_{\underbrace{(ij\dots lm)}_p} \right) = \Pr(\Delta | \mathbf{D}, \mathbf{M}_p)$.

$\Pr \left(M_{\underbrace{(ij\dots lm)}_p} | \mathbf{D}, M_{\underbrace{(ij\dots l)}_{p-1}} \right) = \Pr(\mathbf{M}_p | \mathbf{D}, \mathbf{M}_{p-1})$ is the conditional posterior model probability of

model $M_{\underbrace{(ij\dots lm)}_p}$ at level p under model $M_{\underbrace{(ij\dots l)}_{p-1}}$ at level $p-1$. $\Pr(\mathbf{M}_p | \mathbf{D}, \mathbf{M}_{p-1})$ also represents the conditional model weights and will be used to develop a BMA tree of model weights. Note that model $M_{(ij\dots lm)}$ is a child model under the parent model $M_{(ij\dots l)}$ because both have the same subscript for the first $p-1$ levels. Equation (2) is the Bayesian model averaging (BMA) at level p , which can be written as

$$\Pr(\Delta | \mathbf{D}, \mathbf{M}_{p-1}) = E_{\mathbf{M}_p} [\Pr(\Delta | \mathbf{D}, \mathbf{M}_p)]. \quad (3)$$

According to equations (1) and (3), one can derive the posterior probability of prediction using BMA over models at any level, say level n:

$$\Pr(\Delta | \mathbf{D}, \mathbf{M}_n) = E_{\mathbf{M}_{n+1}} E_{\mathbf{M}_{n+2}} \dots E_{\mathbf{M}_p} [\Pr(\Delta | \mathbf{D}, \mathbf{M}_p)]. \quad (4)$$

Based on equation (4), the law of total expectation and the law of total variance, the prediction mean, within-model variance, between model variance and total variance can be derived at level n.

The hierarch BMA model is the usual BMA model (Hoeting et al., 1999), which is based on equation (1). The hierarch model obtains model averaging results and prediction variances using all base models.

In this study, Δ is the concentration and \mathbf{D} is groundwater head and concentration data used to calibrate groundwater flow and transport models.

Principal Findings and Significance

(1) Saltwater intrusion modeling in the “1,500-foot” sand of the Baton Rouge area

We develop a two-dimensional groundwater flow and mass transport model to predict the saltwater intrusion in the “1,500-foot” sand of the Baton Rouge area. The study area, shown in Figure 1, includes the east-west trending Baton Rouge fault (see Figure 1). The saltwater intrusion model in this report is based on Tsai (2010, 2011). The simulation period is from 1/1/1990 to 12/31/2029 which is divided in calibration part from 1/1/1990 to 1/1/2005 and prediction part from 1/1/2005 to 12/31/2029. The initial groundwater head and the initial chloride concentration are obtained from Tsai (2011). The groundwater model uses the time-varied constant boundary condition for all the boundaries. The mass transport model uses constant concentration in the south boundary. The concentrations in the other boundaries are calculated by the transport simulation model in each time step. The major production wells are Lula pump station and Government Street pump station, which are located north of the Baton Rouge fault. The average pumping rate from Lula pump station is 7.03 million gallons per day and at Government Street pump station is 1.59 million gallons per day. We use MODFLOW (Harbaugh, 2005) and MT3DMS (Zheng and Wang, 1999) to simulate the groundwater flow and mass transport from 1/1/1990 to 12/31/2029. We use 706 head observations from 1/1/1990 to 1/1/2005 at the USGS observation wells shown in Figure 1 to calibrate the model. Then, we develop the prediction models to predict salt water intrusion from 1/1/2005 to 12/31/2029.

(2) Sources of uncertainty and multiple models

We analyze four sources of uncertainty in a hierarchical order in the flow and transport models. They are (1) boundary condition uncertainty, (2) grain-size method uncertainty in determining point-wise hydraulic conductivity, (3) variogram model uncertainty in kriging hydraulic conductivity distribution, and (4) fault permeability architecture uncertainty. To address these sources of uncertainty, 5 boundary condition propositions, three grain-size methods (Kozeny-Carman, Slitcher, and Terzaghi methods), three variogram models (exponential, Gaussian, and spherical), and 3 fault permeability architectures are proposed. This results in $5 \times 3 \times 3 \times 4 = 180$ saltwater intrusion simulation models at the base level of the BMA tree.

In order to track a model in the BMA tree, we use the letter “B” subscribed with percentage of change of boundary head values in the determined boundary condition, the first letter of the grain-size methods, the first letter of the variogram model and the number of fault permeability segments in a hierarchical way to denote a model. For example “B₀KG3” denotes a base model in level 4 that consider no change in the determined boundary condition, Kozeny-Carman method, the Gaussian variogram and three-segment fault permeability architecture. “B₀KG” is a BMA model at level 3 that averages base models with different fault permeability architectures given “B₀” boundary condition, “K” grain-sized method and “G” variogram model propositions. “B₀K” is a BMA model at level 2 that averages level-3 BMA models with different grain-size method propositions given “B₀” boundary condition proposition. “B₀” is a BMA model at level 1 that averages level-2 BMA models with different variogram model propositions given “B₀” boundary condition and “K” grain-sized method propositions.

(3) BMA Tree of model weights

Figure 2 shows the BMA tree of model weights in parentheses and conditional model weights. The model weights reflect the comparative importance of all the competitive modeling propositions in one level. The conditional model weights represent the relative importance of the different propositions under the same parent models. The base level of the BMA tree corresponds to different fault permeability segments. The simulation models using homogeneous fault permeability can be discarded because they provide very poor fitting to the observation data and are not shown in the BMA tree.

At the base level, the best base model is B₀KG3 with the model weight 20.41%. At the third level, the BMA models are developed by averaging concentration predictions from their child base models that use different fault permeability architectures. The “B₀KG” is the best model with model weight 38.93% the second best model is the “B₀KS” with model weight 28.75%. The relative model weights show that the ranking of the variogram models is the same under both “B₀K” and “B₊₁₀K” models. The Gaussian model is a better proposition than the spherical and exponential models to determine the hydraulic conductivity distribution.

At the second level, BMA models are developed by averaging concentration predictions from their child BMA models that use different variogram models for hydraulic conductivity estimation. As shown in Figure 2, since Terzaghi and Slitcher methods have significantly worse fit to the observation data, only Kozeny-Carman method are remained at the second level. The “B₀K” model weight is 78.64% and the “B₊₁₀K” model weight is 21.36%. Their conditional model weights are 100% under their parent model.

At the first level, BMA models are developed by averaging concentration predictions by their child BMA models that use different grain-size methods. However, from previous analysis, we found that only Kozeny-Carman method was left to be used. At this level the determined boundary condition (B₀) is dominantly the best model with the model weight 78.64% and B₊₁₀ is the second best model with model weight 21.36%. Other boundary condition propositions are discarded because of poor fitting to the observation data.

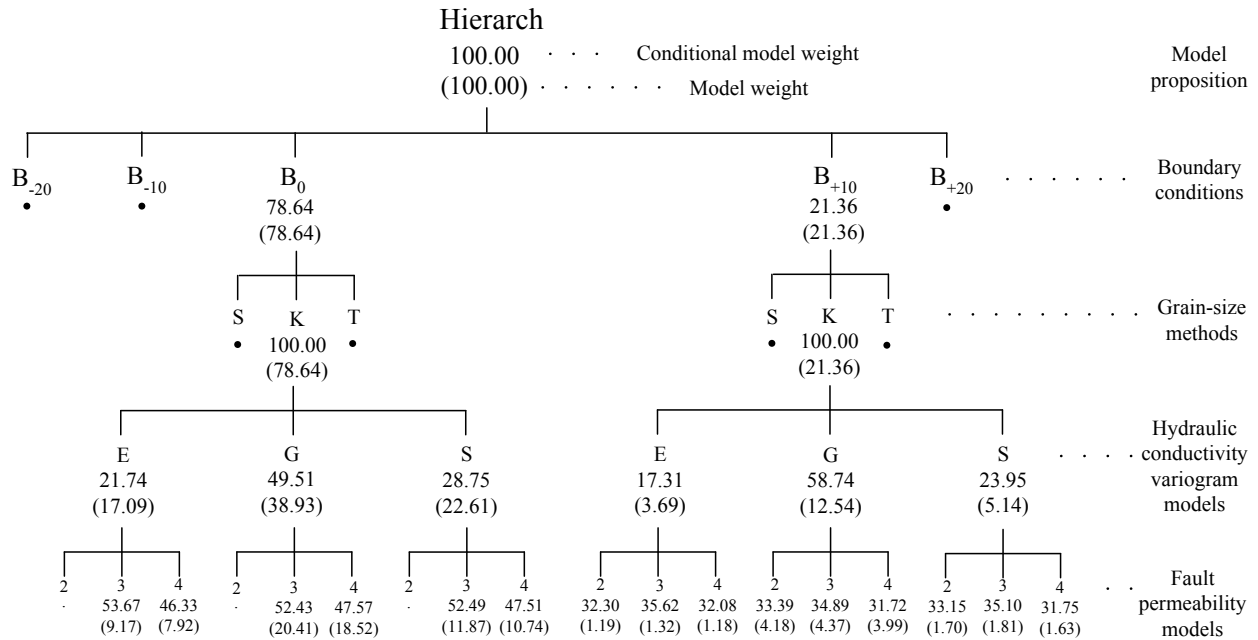
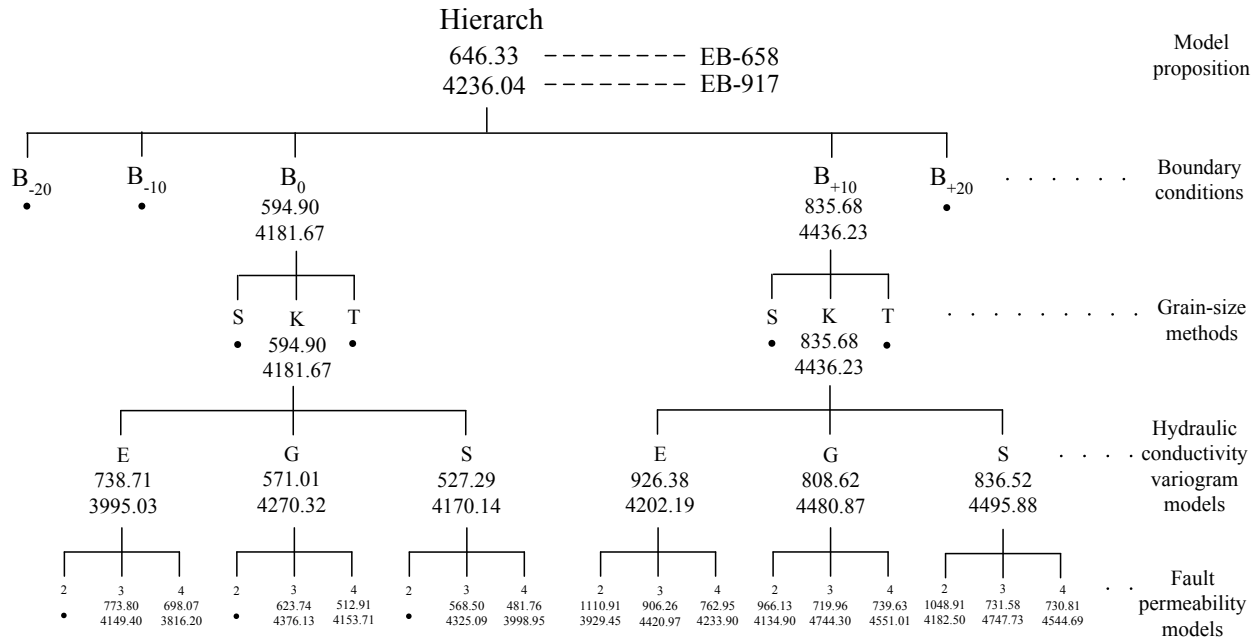


Figure 2: BMA tree of model weights and conditional model weights.

(4) BMA tree of mean concentration predictions

The BMA tree of mean concentration predictions for the EB-658 and the EB-917 on 12/31/2029 is shown in Figure 3. The predicted mean concentration at EB-658 at the base level is between 481.76 mg/L and 1110.91 mg/L and. The predicted mean concentration at EB-917 at the base level is between 3816.20 mg/L and 4747.73 mg/L. The mean concentration prediction range becomes narrower while going up to upper layers because of the nature of averaging and the reduction in the number of models. At the level 3 the mean concentration range at EB-658 is between 527.29 mg/L and 926.38 mg/L and the mean concentration range at EB-917 is between 3995.03 mg/L and 4495.88 mg/L. At the level 2 and level 3, the concentration prediction range for EB-658 is between 594.90 mg/L and 835.68 mg/L and for EB-917 is between 4181 mg/L and 4436.23 mg/L. The hierarch BMA model predicts mean concentration at EB-658 and EB-917 is 646.33 mg/L and 4236.04 mg/L. It was found that all of the models with 3-segment fault proposition predict higher mean concentration at EB-917 than the models with 2-segment or 4-segment fault proposition.

The BMA tree of mean predictions shown in Figure 3 provides an understanding of mean prediction variability over the accumulation of sources of uncertainty, which is not possible to know via the traditional BMA method.



PR

Figure 3: BMA tree of mean concentration predictions (mg/L) at the EB-658 and EB-917 at the 12/31/2029.

(5) Temporal predictions and variances

Figure 4 shows the EB-917 concentration predictions and the one standard deviation bound using models at the different levels for the prediction period. All of the models predict the increasing concentration at EB-917. As shown in Figure 4, none of the USGS chloride data is inside the one standard deviation bound of the B₀KG3 base model and B₀KG model. Two chloride data are in one standard deviation bound of the B₀K and B₀ models and all chloride data are in the one standard deviation bound of the hierarchy model.

According to Figure 4, it is clear to see that prediction variance caused by uncertain model parameters is much smaller than that caused by different model propositions. Moreover, the prediction variances at all levels start to increase at the beginning of time and then decrease. This behavior is reasonable because at early time all models predict similar low concentration at EB-917. Therefore the prediction variances are small. High prediction variances occur due to predicting concentration quite differently by different models. At later time all models start to predict similar high concentration at EB-917. Therefore, prediction variance decreases. The hierarchy model has much higher prediction variance comparing to the B₀ model is because it includes high prediction variance from the B₊₁₀ model.

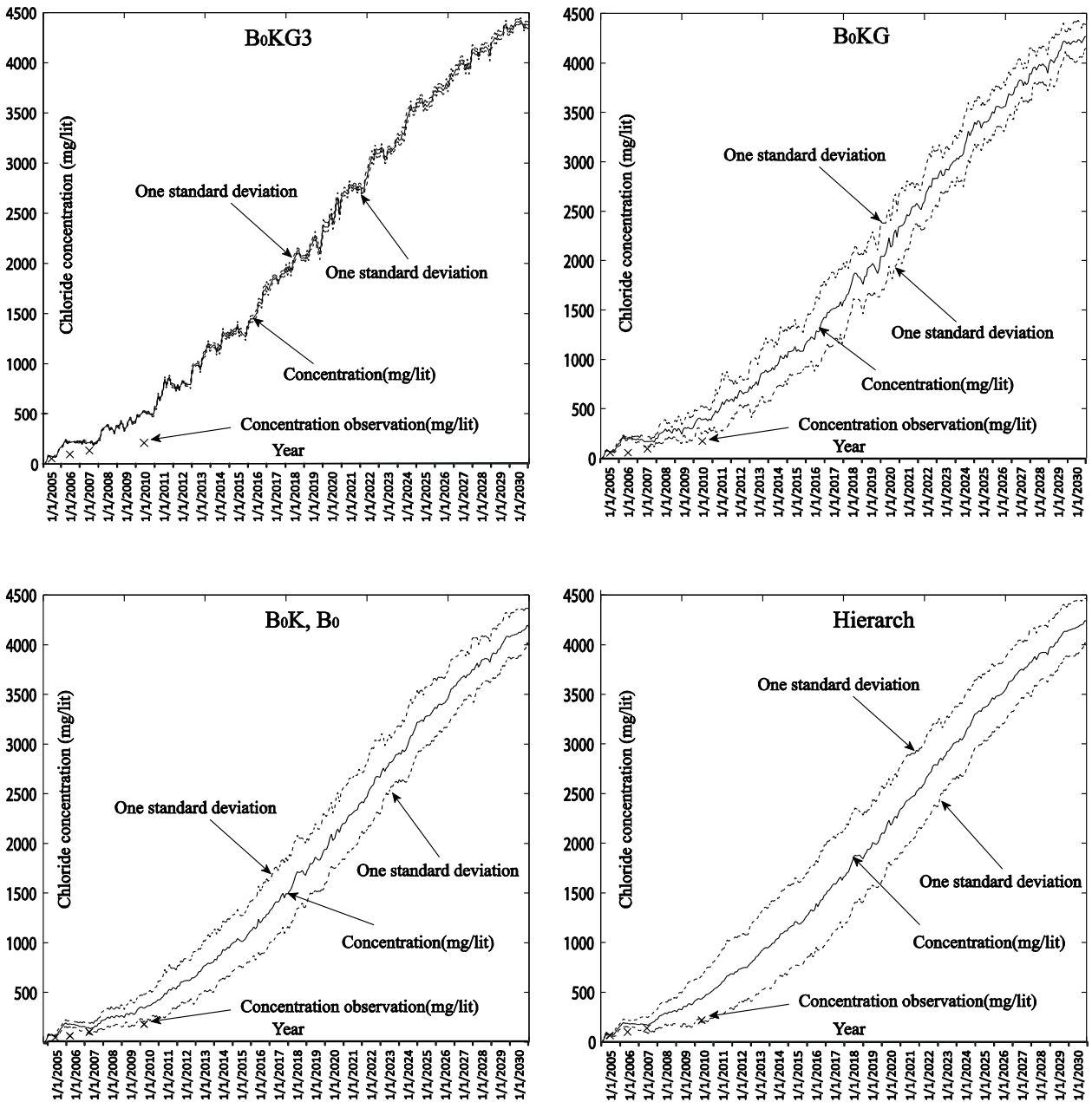


Figure 4: One standard deviation error bound of predicted concentration at EB-917 from 1/1/2005 to 12/31/2029. Crosses are USGS chloride data.

References

Chitsazan, N. and F. T.-C. Tsai, Hierarchical Bayesian model averaging for chance constrained remediation designs, H33I-1450 Abstract, 2012 American Geophysical Union Fall Meeting, San Francisco, CA, 3-7 December 2012.

Harbaugh, A.W. 2005. MODFLOW-2005: the U.S. Geological Survey modular ground-water model-The ground-water flow process: U.S. Geological Survey Techniques and Methods 6-A16.

- Hoeting, J.A., D. Madigan, A.E. Raftery, and C.T. Volinsky. 1999. Bayesian model averaging: A tutorial. *Statistical Science*, 14(4), 382-401.
- Sargent, B.P. 2012. Water use in Louisiana, 2010, Louisiana Department of Transportation and Development, Water Resources Special Report No. 17 (Revised).
- Tsai, F.T.-C. 2010. Bayesian model averaging assessment on groundwater management under model structure uncertainty. *Stochastic Environmental Research and Risk Assessment* 24(6), 845-861.
- Tsai, F.T.-C. 2011. Scavenger well operation model to assist BRWC to identify cost-effective approaches to stop saltwater intrusion toward the BRWC water wells in the “1,500-foot” sand of the Baton Rouge area. Technical report to Baton Rouge Water Company and Capital Area Groundwater Conservation Commission, Louisiana.
- Tsai, F.T.-C. and A. S. Elshall. 2013. Hierarchical Bayesian model averaging for hydrostratigraphic modeling: Uncertainty segregation and comparative evaluation, *Water Resources Research*, 2013. (accepted)
- Zheng, C. and P.P. Wang. 1999. MT3DMS—A modular three-dimensional multispecies transport model for simulation of advection, dispersion and chemical reactions of contaminants in ground-water systems; documentation and user’s guide: Jacksonville, Fla., U.S. Army Corps of Engineers Contract Report SERDP-99-1, 221p.

6. Student Support

- Nima Chitsazan, PhD student
- Ehsan Beigi, PhD student
- Ahmed Elshall, PhD student
- Elizabeth L. Chamberlain, MS student

Nutrient and harmful algal bloom (HAB) dynamics in Lake Pontchartrain during a non-spillway opening year

Basic Information

Title:	Nutrient and harmful algal bloom (HAB) dynamics in Lake Pontchartrain during a non-spillway opening year
Project Number:	2012LA83B
Start Date:	3/1/2012
End Date:	2/28/2012
Funding Source:	104B
Congressional District:	6th
Research Category:	Biological Sciences
Focus Category:	Water Quality, Surface Water, Ecology
Descriptors:	None
Principal Investigators:	John R White, Sibel Bargu, Chunyan Li

Publications

1. Roy ED, White JR, Smith EA, Bargu S, Li C. Estuarine ecosystem response to three large-scale Mississippi River flood diversion events. *Science of the Total Environment* 2013;458-460:374-387.
2. Controls on Microbial Processing of Nitrate in Floodwaters during Large-Scale Diversions of Mississippi River Water. *J.R. White and E. Roy. Invited Oral Presentation at the Annual Meeting of the Society of Wetland Scientists, (June 2-4, 2013) Duluth, MN.
3. Estuarine Ecosystem Response to Three large-scale Mississippi River Flood Diversion Events Roy, E. D., White, J. R., Smith, E., A., Bargu, S., Li, C. Oral Presentation at the ASLO Ocean Sciences Meeting (Feb 2013) New Orleans, LA.
4. Nutrient Dynamics at the Estuarine Sediment-Water Interface during Large Pulses of High Nitrate Mississippi River Water. E.D. Roy and J.R. White. Oral Presentation at the 9th INTECOL International Wetlands Conference (June 2012) Orlando, FL.

Problem and Research Objectives

Phytoplankton are considered to be one of the major primary producers in estuaries that support the diversity and productivity. As estuaries become increasingly subject to higher loads of bioavailable nutrients, eutrophic conditions may become more pronounced shown by high algal production, hypoxia and associated fish kills. During the past five years, the Bonnet Carré spillway has been opened twice (2008, 2011) to mitigate potential flooding to the City of New Orleans and downstream communities. In doing so, a volume of Mississippi River water greater than the volume of the entire lake has been diverted into Lake Pontchartrain along with a very large nutrient load (100s to 10,000s of metric tons of P and N, respectively). In Lake Pontchartrain, both non-toxic and toxic phytoplankton blooms occurred after the 1997 and 2008 Bonnet Carré Spillway openings. Toxic cyanobacteria dominance and their associated toxins were present and varied over time and space threatening the ecosystem (Dortch & Achee, 1998; Bargu et al. 2011).

The effect of these large nutrient and hydraulic fluxes has been studied by the current research team by funding through the National Science Foundation. However, there are no programs/funds available to document the “non-spillway” or background conditions of the lake, especially along the east-west axis of the lake coincident with the salinity gradient. In order to determine the effects of these large nutrient loads on lake water quality, we need to undertake a spatially and temporally explicit field sampling campaign spanning from March – October 2012 to determine water quality including nutrient concentrations, algal toxins and phytoplankton population measures.

The health of Lake Pontchartrain is important to the economy of Louisiana, specifically related to the fisheries. It is imperative to understand the triggers to harmful algal blooms as the associated toxins have the potential to contaminate the entire food web. In order to assess the causes of potential animal mortality and morbidity and its potential link to harmful algal toxins, generating baseline datasets such as the one proposed here is fundamental and necessary as a baseline or point of reference for future research. The findings from this proposal will be shared immediately with the Department of Health & Hospitals – Office of Public Health, and Louisiana Department of Environmental Quality.

The specific objectives include:

- (1) Determining baseline dissolved N and P concentrations over time and space
- (2) Quantifying cyanotoxin concentration correlated to phytoplankton assemblages over time and space.
- (3) Combining data from this effort (non-spillway year) with data from two previous annual sampling campaigns (spillway years) to build a simple ecosystem model on how spillway opening can potentially affect the water quality and health of the fisheries in Lake Pontchartrain.

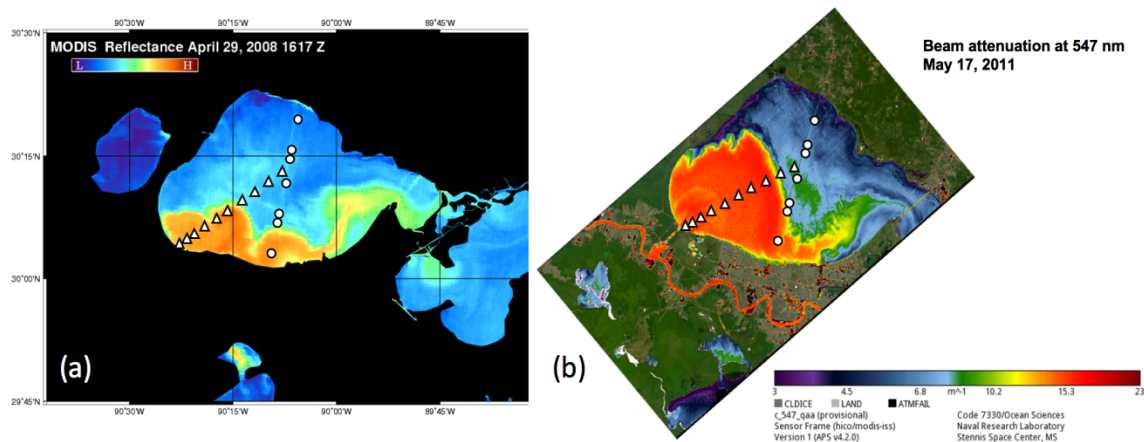


Figure 1. MODIS satellite imagery of Lake Pontchartrain on (a) April 29, 2008 and (b) May 17, 2011 provided by the LSU Earth Scan Laboratory and the US Naval Research Laboratory at the Stennis Space Center in Mississippi, respectively. Orange or red tones depict sediment-laden Mississippi River water (measured as red band reflectance in 2008 and beam attenuation at 547 nm in 2011). Blue tones depict estuarine water and land is colored black and green/brown in the 2008 and 2011 images, respectively. The 10 stations shown as Δ comprise the 30-km transect used in this and past studies (White et al. 2009; Bargu et al. 2011). The 7 stations shown as \circ were sampled by Turner et al. (2004) in 1997.

Methodology

We conducted 7 sampling trips from March to August 2012, focused on the springtime bloom period and the late summer period when HABs have been detected in the Lake Pontchartrain. We sampled three stations spanning in 2012 the length of our previously established a 10-station, 30 km transect in the western portion of the lake during the spillway years (Figure 1). In addition, in 2011, we added stations in the eastern half of the lake including stations at the two outlets to the Gulf of Mexico, The Rigolets and Chef Menteur passes. That sampling schedule gave us excellent spatial coverage along the east-west axis of the lake from the more saline section to the less saline western boundary (Figure 1). In 2012, we focused on the 3 transect stations along with 4 stations in the northwest quadrant of the estuary where cyanobacteria have been previously observed. Additionally, we sampled upstream of the confluences of Pass Manchac, the Tangipahoa River, and the Tchefuncte River with Lake Pontchartrain to help gauge contributions of nutrients and biology from the North Shore.

Water samples were collected at all stations (minimum of 15 spanning the lake) at 10 cm below the surface (to avoid floating debris and hydrophobic films) and at 1 m from the bottom at transect stations. Our experience during the spillway events has shown that other than dissolved oxygen, there were no differences in water quality and water chemistry between the surface and deep stations, primarily due to the turbulence produced by the spillway. However, during the non-spillway years, we will sample both depths to document any stratification. At each station, the secchi disk depth will be recorded, salinity, temperature, DO, and pH will be taken with a YSI handheld meter and turbidity and phycocyanin pigment measurements were taken using a handheld Turner fluorometer. Four discrete water samples were at each depth for each station; 1L sample for total suspended solids (TSS), 125 mL bottle for total nutrients, 30 mL field-filtered sample for dissolved inorganic nutrients, and a 1 L bottle for chlorophyll measurements and characterization of the phytoplankton community. Preliminary examinations of the

phytoplankton community revealed species of cyanobacteria capable of producing the cyanotoxins MCs, saxitoxin, anatoxin and cylindrospermopsin in the Lake Pontchartrain (Bargu et al. 2011). MCs are commonly detected toxins in the lake and they can be produced by both *Microcystis* and *Anabaena*, two most common toxic species previously observed in the lake (Bargu et al. 2011).

Laboratory Analyses

Nutrient Analyses. Filtered water samples were analyzed for dissolved Si, NH₄, NO₃ and DRP on a Seal Analytical Discrete Colorimetric analyzer (USEPA, 1993). DOC and DON were analyzed on a Shimadzu TOC/TN analyzer. Unfiltered samples underwent acid digestion and then analyzed for TKN and TP.

Total Suspended Solids: Total Suspended Solids and Total Volatile Solids were determined within 24 hours by filtration through pre-ashed and pre-washed glass fiber filters, dried and weight for TSS. Then samples were ashed at 550 C for 4 hours and reweighed to determine weight percent volatile solids (APHA, 2540 D and E/G).

Chlorophyll *a* (*chl a*) and Microscopy Analyses. Chlorophyll *a* were determined for all stations as a measure of phytoplankton biomass using a Turner fluorometer (Model 10-AU) following the protocol from Parsons et al. (1984). Subsamples preserved with 2% glutaraldehyde and kept in a dark, at room temperature were used to determine the species composition of the phytoplankton community using an inverted microscope (Axiovert 135, Zeiss).

Phycotoxin Measurements. Water samples were analyzed for the cyanobacteria toxins, microcystin and cylindrospermopsin, using Enzyme-Linked Immunosorbant Assay (ELISA) with a detection limit of 0.10 µg l⁻¹. Samples were analyzed following the protocols included in the ELISA kits (Abraxis, LLC).

Lake Hydrodynamics

Hydrodynamic and hydrographic data will be used to help the interpretation of the distribution of nutrients and the bio-chemical characteristics of the lake. A long time series of hydrodynamic and hydrographic data has been collected in the lake during several projects funded by NSF after Hurricane Katrina, the 2008 and 2011 flood and Bonnet Carré Spillway opening. These include current velocity profiles, water level, and water temperature and salinity from the tidal channels (Rigolets, Chef, and Industrial Canal). Data from along the causeway also were collected for water level, water temperature, and salinity. Numerous ship based surveys were also conducted in the Lake at various locations and along many transects. These shipboard measurements will be repeated during each sampling cruise.

Principal Findings and Significance

Comparative Analysis of Spillway Openings

This work was compiled into a manuscript, submitted for review, accepted, and published during the funding period (Roy et al. 2013). The two spillway events analyzed were all characterized by the discharge of a volume of Mississippi River water greater than the total volume of Lake Pontchartrain. The 2011 opening had the largest total discharge (21.9 km³) and occurred later than the events in 2008 (7.5 km³). Discharges in 2008 and 2011 were equal to 113% and 330% of Lake Pontchartrain's volume, respectively (Table 1).

Table 1. Physical characteristics, nitrate (NO_x-N) plume collapse times, and phytoplankton dynamics in Lake Pontchartrain during the Bonnet Carré Spillway inflow events in 2008 and 2011.

	2008	2011
% of Lake Volume Discharged by Spillway	113 ^a	330
Day Spillway Closed	9-May	20-Jun
NO _x -N Plume Collapse Time (d)	21 ^b	21
Date of Full NO _x -N Plume Collapse	30-May	11-Jul
Max Chl <i>a</i> (µg/L)	58 ^c	45
CyanoHAB Observed	Yes ^c	No
Date CyanoHAB Detected	21-May	-

^aWhite et al. (2009). ^bBargu et al. (2011), ^cFrom surface algal bloom.

The greater discharge in 2011 resulted in a near-linear increase in the sediment-rich freshwater plume area to a maximum of 1241 km² 14 days post-opening in comparison to the 616 km² plume observed by White et al. (2009) in 2008 (Figure 3). The maximum turbid freshwater plume areas in 2008 and 2011 were equal to 38% and 76% of the total surface area of Lake Pontchartrain, respectively. Sediment-rich water was observed exiting Lake Pontchartrain via both of its eastern outlets in satellite imagery on May 23, 2011, indicating that the leading edge of the turbid freshwater plume traveled across the estuary in ≤ 14 days in 2011. As in 2008 (White et al., 2009), the leading plume edge in 2011 initially traveled along the southern edge of Lake Pontchartrain (Figure 1).

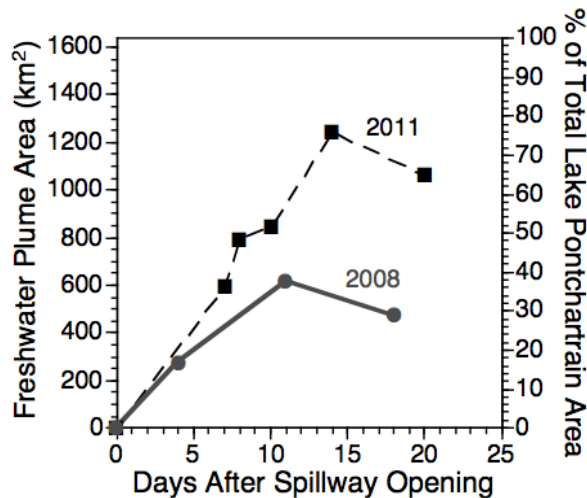


Figure 3. Area of sediment-rich freshwater plume in Lake Pontchartrain as a function of time identified using satellite imagery from the LSU Earth Scan Laboratory during the Bonnet Carré Spillway events in 2008 (White et al. 2009) and 2011 (this study).

Salinity (Figure 4) and surface water temperature (Figure 5) dynamics in 2008 are described in detail in White et al. (2009) and Bargu et al. (2011). In 2011, salinity in Lake Pontchartrain across the sample transect ranged from 2.6-4.9 PSU on May 8th prior to the 2011 spillway opening (Figure 4). Lower salinities at stations closest to the spillway indicated leakage of Mississippi River water through the spillway prior to its opening. Salinity on May 18, 2011 was

≤ 0.15 PSU at all stations except the two furthest from the inflow (0.79-2.72 PSU) during the spillway opening (Figure 4). Fluctuations in salinity occurred at the three stations furthest from the inflow through June 16, 2011. Surface water temperature was > 20.0 °C at all stations on May 18, 2011 and increased to > 28.2 °C at all stations by June 16, 2011 (Figure 5). Following spillway closure on June 20th, salinity averaged 0.34 PSU across the transect on June 21st and remained below 1.2 PSU at all stations through July 11th during the nitrate collapse period with evidence of slow dilution by estuarine water (Figure 4). Surface water temperatures were > 29.0 °C at all stations during the nitrate collapse period in 2011 (Figure 5). On August 10, 2011 salinity remained ≤ 1.2 PSU at all stations, indicating a much slower rate of salinity increase following spillway closure than observed in 2008 by Bargu et al. (2011) (Figure 4). Post-nitrate collapse surface water temperatures in 2011 were > 28.7 °C at all stations (Figure 5).

Nutrient loading to Lake Pontchartrain during the three events was correlated to discharge (Table 2). In all two events, the DIN pool in spillway inflow was consistently dominated by NO_3^- with total $\text{NO}_x\text{-N}$ loads of 9714 and 25395 Mg in 2008 and 2011, respectively. In general nutrient loads were 2.6-3.5 times greater in 2011 than in 2008. For both events the DIN:DIP molar ratio of spillway inflow waters ($\geq 50:1$) was well above the Redfield ratio of 16:1, indicating potential for eventual P limitation of primary production. The DSi:DIN molar ratio of spillway inflow was near or greater than 1:1 for all events.

Table 2. Nutrient loads to Lake Pontchartrain from the Bonnet Carré Spillway in 2008 and 2011. The final column shows 2011 loads divided by 2008 loads.

	2008	2011	2011/2008
Nitrate+Nitrite (Mg $\text{NO}_x\text{-N}$)	9714 ^a	25395	2.6
Ammonia (Mg $\text{NH}_4\text{-N}$)	224 ^a	690	3.1
DIN (Mg N)	9938 ^a	26085	2.6
DIP (Mg P)	400 ^b	1122	2.8
DSi (Mg Si)	19347	67319	3.5
DSi:DIN:DIP Inflow Molar Ratio	57:59:1	63:50:1	-

^aBased on values reported in White et al. (2009). ^bRoy et al. (2012)

Secchi depth in Lake Pontchartrain ranged from 0.8-1.2 m on May 8, 2011 prior to the 2011 spillway opening and decreased to 0.2-0.6 m during the spillway opening (Figure 6). Following spillway closure on June 20, 2011, Secchi depth increased to as high as 3.4 m in July under NO_3^- depleted conditions and remained > 0.76 m at all stations through August with several measurements > 2 m (Figure 6).

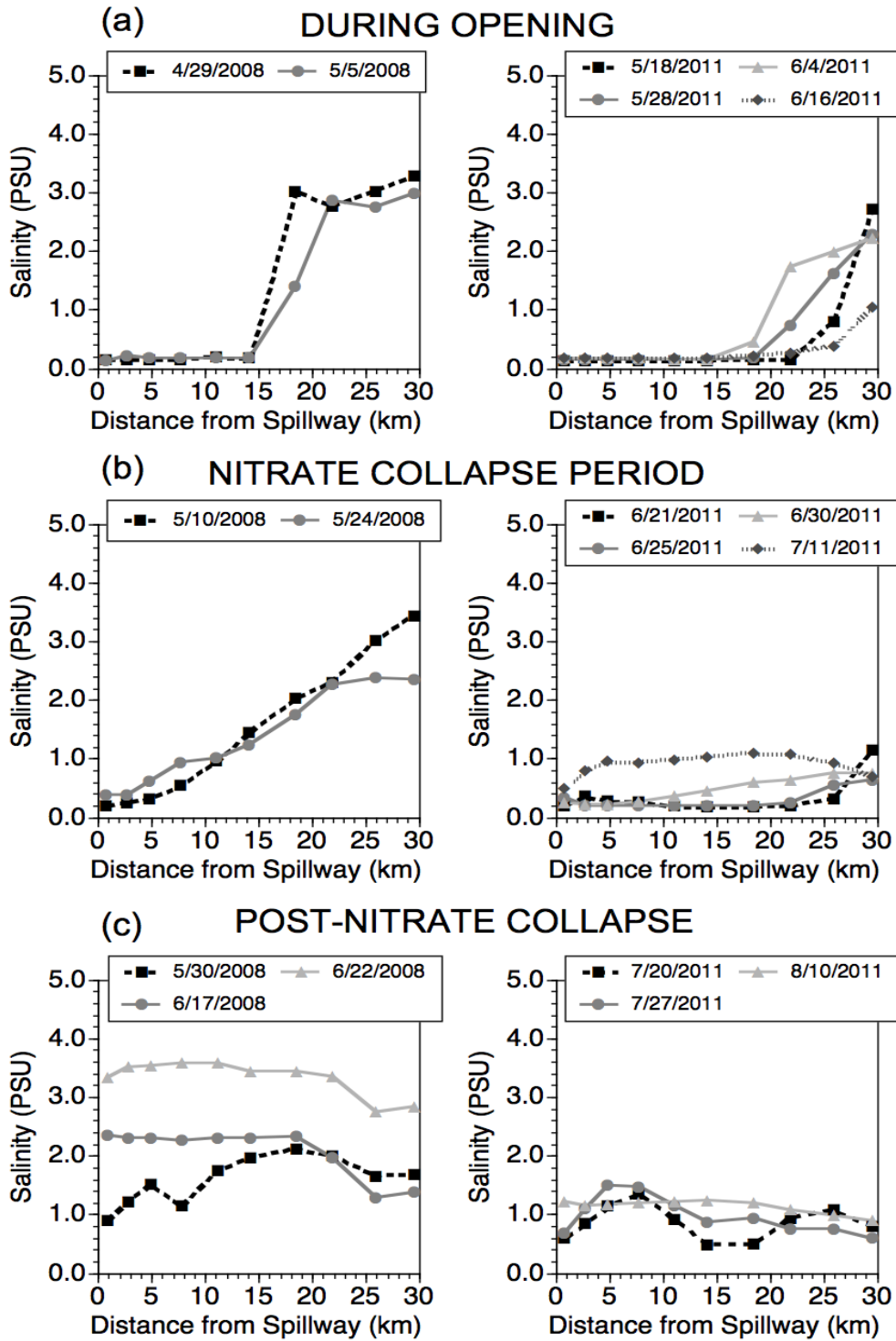


Figure 4. Salinity along the 30-km 10-station study transect (Fig. 1, Δ) during (a) the spillway opening, (b) nitrate collapse, and (c) post-nitrate collapse periods in 2008 (left panel) and 2011 (right panel). 2008 data are from White et al. (2009) and Bargu et al. (2011).

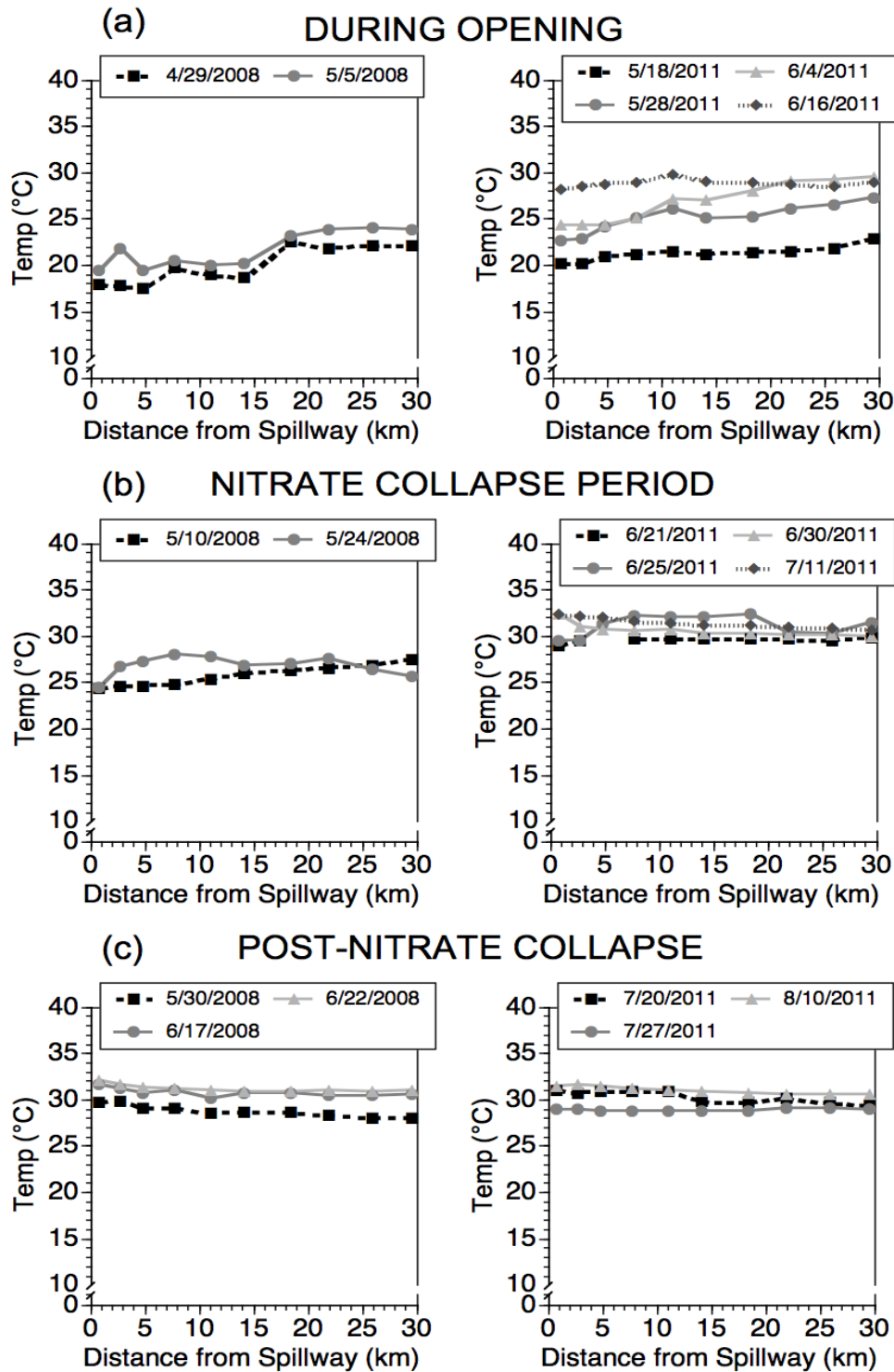


Figure 5. Surface water temperature along the 30-km 10-station study transect (Fig. 1, Δ) during (a) the spillway opening, (b) nitrate collapse, and (c) post-nitrate collapse periods in 2008 (left panel) and 2011 (right panel). 2008 data are from White et al. (2009) and Bargu et al. (2011).

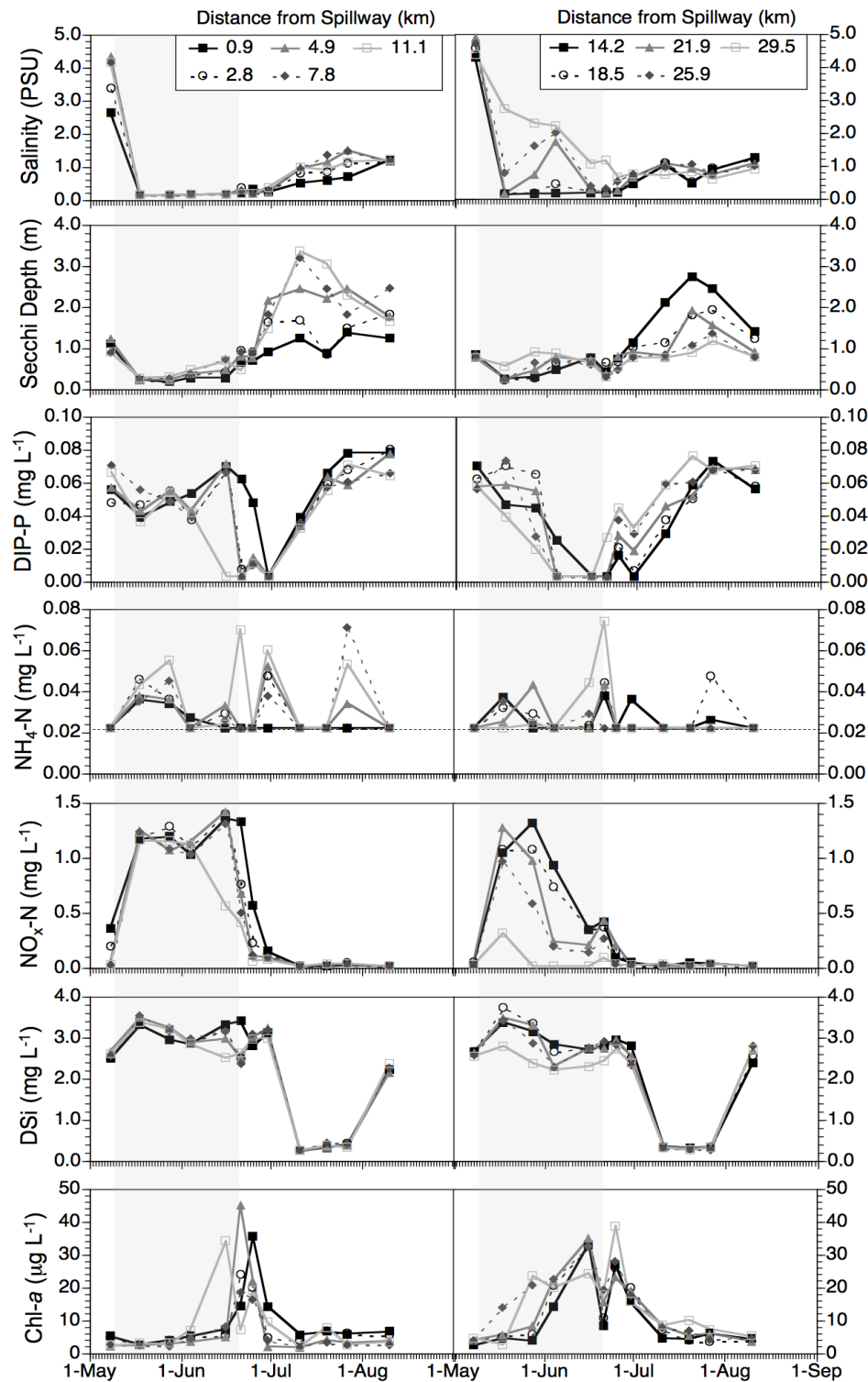


Figure 6. Salinity (PSU), Secchi depth (m), dissolved inorganic phosphorus (mg DIP-P L⁻¹), ammonium (mg NH₄-N L⁻¹), nitrate (mg NO_x-N L⁻¹), dissolved silica (mg DSi L⁻¹) and chlorophyll-*a* (µg L⁻¹) across the 30-km 10 station transect in Lake Pontchartrain extending from the Bonnet Carré Spillway inflow (0.9 km) to the lake center (29.5 km) (Fig. 1, Δ). The left and right panels show stations 0.9-11.1 km and 14.2-29.5 km from the spillway inflow, respectively. The shaded regions indicate the period during which the spillway was open (May 9 – June 20). Dotted lines in the NH₄-N plots indicate the detection limit.

Nitrate concentrations on May 18, 2011 in the Mississippi River plume ranged from 1.04-1.27 mg NO_x-N L⁻¹ (Figure 6). During this time, NO₃⁻ concentrations remained ≥ 1 mg NO_x-N L⁻¹ at stations with salinity ≤ 0.2 PSU except on June 16th when concentrations began to decline. Nitrate concentrations decreased rapidly following spillway closure and by July 11th, NO_x-N concentrations were below detection (detection limit = 0.016 mg L⁻¹) at all stations except the two furthest from the spillway inflow (0.03-0.04 mg L⁻¹) (Figure 6), indicating a NO₃⁻ plume collapse time of 21 days (Table 1). Nitrate concentrations largely remained below 0.04 mg NO_x-N L⁻¹ at all stations through August. NH₄-N concentrations were often below detection (< 0.022 mg L⁻¹) and never increased above 0.07 mg L⁻¹ throughout the spillway opening and post-closure period (Figure 6).

The mean measured DIP-P concentration was 0.054 mg L⁻¹ in spillway inflow waters. Water column DIP concentrations decreased rapidly in Lake Pontchartrain between June 4th and June 30th with depletion occurring earlier with increased distance from the spillway due partially to dilution (Figure 6). Following DIP depletion across the entire transect post-spillway closure, concentrations rebounded at all sites and by July 27th were greater than the concentration of loaded Mississippi River water at all stations.

Water column DSi concentrations were near or above 3 mg L⁻¹ within the Mississippi River plume during the opening, before rapidly decreasing below 0.5 mg L⁻¹ between June 30th and July 11th (Figure 6). DSi concentrations remained low before increasing rapidly between July 27th and August 10th to > 2 mg L⁻¹.

On May 8, 2011, Chl *a* values were relatively low (2.32-10.26 μg L⁻¹) and then increased during the spillway opening at the outer most stations (5.67- 34.13 μg L⁻¹) (Figure 6). Results indicate that low light availability (measured as Secchi disk depth) corresponded to low phytoplankton biomass (measured as Chl *a*) within the sediment-rich Mississippi River plume near the spillway inflow despite available nutrients. Immediately following spillway closure, the Chl *a* concentration reached a maximum of 45.09 μg L⁻¹ on June 21st at 4.9 km from the spillway inflow. Chlorophyll peaks corresponded to depletion of NO₃⁻ and DIP of Mississippi River origin (Figure 6). Chlorophytes were the dominant phytoplankton group at the time and location of maximum Chl *a* and accounted for a spatial average of 52-76% of the phytoplankton group composition during the period of greatest Chl *a* (June 16th, 21st, and 25th) (Figure 7). Cyanobacteria accounted for a spatial average of 7-22% of the group composition during this period. Phytoplankton biomass declined after June 25th and by July 11th Chl *a* concentrations were < 8.55 μg L⁻¹ at all sites. No increases in biomass were observed from this time through the final sampling on August 10th (Figure 6).

The observed times for NO₃⁻ plume collapse following spillway closure were identical in 2008 and 2011 at 21 days (Table 1).

Dominance of the phytoplankton community by CyanoHAB species was observed in 2008 (May 21st, Bargu et al., 2011) following closure of the spillway, but not in 2011 (Figure 7). Maximum Chl *a* concentrations were 58 and 45 μg L⁻¹ for 2008 and 2011, respectively. The 2008 CyanoHAB occurred within 2 weeks of closure (Table 1).

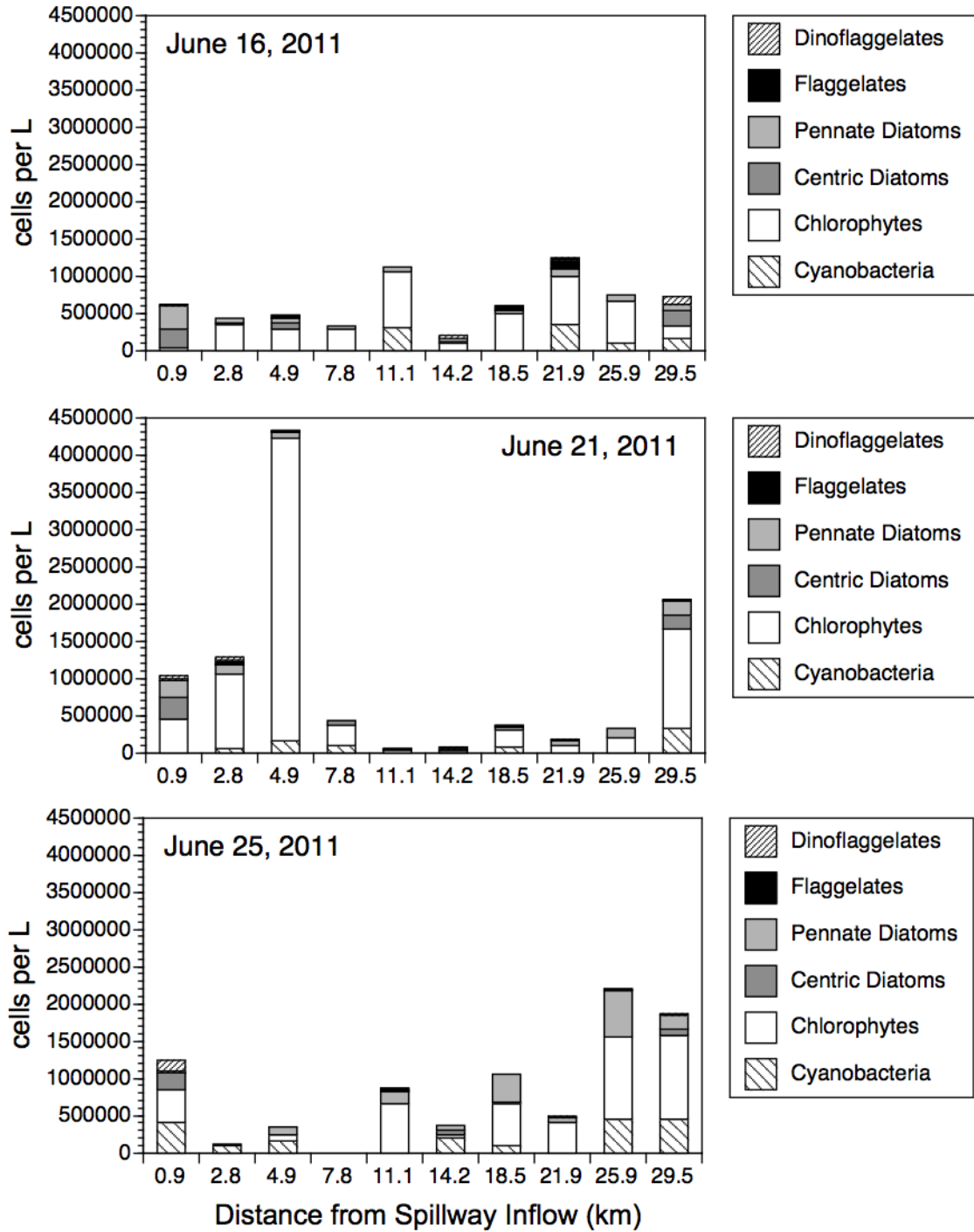


Figure 7. Phytoplankton group composition across the 30 km transect extending northeast from the Bonnet Carré Spillway inflow (Fig. 1, Δ) during the period of increased Chl *a* observed following the 2011 opening.

The Bonnet Carré Spillway events analyzed here had closures in May (2008) and June (2011) (Figure 2). The 30-d time period following closure in 2011 was characterized by significantly ($P < 0.01$) lower daily mean wind speed and significantly ($P < 0.01$) higher daily mean air temperature than those in 2008 (Table 3).

Table 3. Weather and Lake Pontchartrain surface water characteristics during the period following the closure of the Bonnet Carré Spillway in 2008 and 2011. Weather data is from the National Climatic Data Center (Louis Armstrong New Orleans Int'l Airport). Letters indicate significant differences ($P < 0.01$) in weather characteristics for different time periods.

Year	2008	2011
Days After Spillway Closure	1 - 30	1 - 30
Daily Mean Wind Speed (m s^{-1})	3.6 ± 1.1^b	2.9 ± 1.1^c
Daily Mean Air Temp. ($^{\circ}\text{C}$)	26.0 ± 2.2^a	28.9 ± 1.2^b

*From Bargu et al. (2011).

The immense rate of freshwater discharge through the Bonnet Carré Spillway during diversions (up to nearly $9000 \text{ m}^3 \text{ s}^{-1}$ in 2011, Figure 2) results in a relatively rapid expansion of a freshwater plume that can impact a significant portion of Lake Pontchartrain (Figures 3 and 4). The plume is characterized horizontally by a narrow ($< 10 \text{ km}$) edge of mixed fresh and estuarine water (Figure 4) and is vertically well mixed (White et al., 2009). Essentially, the plume behaves as a river flowing through the shallow estuary during the inflow event. The tendency for the plume waters to travel along the southern rim of the estuary is driven by the Coriolis effect, but can also be impacted by wind (White et al., 2009). Plume waters near the spillway during the opening are characterized by high suspended sediments (White et al., 2009) and low Secchi depth (Figure 6). Phytoplankton biomass (represented here as Chl *a*) in this region of the freshwater plume is therefore limited by light availability despite readily available nutrients (Figures 6 and 8). The high discharge rate creates a turbulent, horizontally dynamic, and vertically well-mixed environment in the region near the spillway, likely also depressing primary productivity (Figure 8).

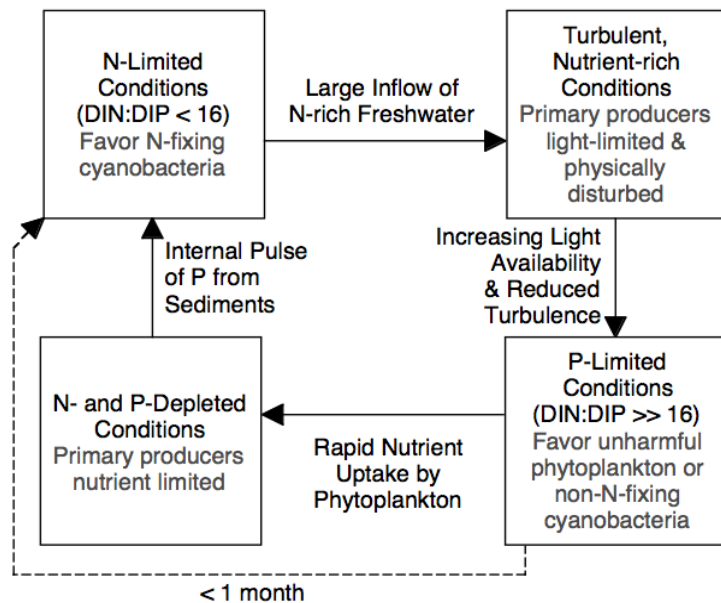


Figure 9. Estuarine biogeochemical dynamics during large inflows of nitrate-rich freshwater. Diagram is based on observations in Lake Pontchartrain during the 2008 and 2011 Bonnet Carré Spillway openings. Dotted line indicates that the system can move from P-limitation to N-limitation in < 1 month.

As light limitation is alleviated and physical disturbance decreases, either in regions more distant from the spillway during the opening or following spillway closure, phytoplankton rapidly compete for a one-time N-rich nutrient-boon (Figures 6 and 8). Continued freshwater inflow causes continued horizontal displacement of water in regions further from the spillway despite less turbulent and turbid conditions, resulting in outflow to the coastal ocean (Figure 1). Previous research has shown that cyanobacteria exhibit greater relative biomass when flushing is minimal (i.e., less horizontal displacement of the water column) (Paerl, 2006). Therefore, the river-like nature of the flowing freshwater plume during spillway events likely provides a competitive advantage for diatoms and chlorophytes.

Temperature and wind are two physical factors that may influence phytoplankton community composition during the period of rapid nutrient assimilation and peak phytoplankton biomass. Cyanobacteria generally exhibit greater growth rates at high surface water temperatures (> 25°C) than diatoms, although chlorophytes also achieve maximum growth rates at > 25°C (Paerl et al., 2011). Diverted Mississippi River water that is cooler than resident estuarine water quickly warms in the estuary as air temperatures increase (Figure 5). Not surprisingly, diversion timing impacts temperature dynamics. The earlier diversion period in 2008 resulted in surface water temperatures of 24-28°C during the nitrate collapse period in comparison to 28-32°C in 2011 (Figure 5).

Lake Pontchartrain is an exposed, wind-dominated estuary and wind-induced turbulence and turbidity can limit cyanobacterial success in estuaries due to disruption of vertical stratification and surface bloom formation (Paerl, 2006). However, our results showing that daily mean wind speeds were significantly lower for the 30 days following spillway closure in 2011 in comparison to periods in 2008 when CyanoHABs were observed (Table 3) suggest that wind-wave action was not the dominant factor responsible for the absence of cyanobacterial dominance in 2011 (Table 3).

Following spillway closure, mixing of estuarine water with the freshwater plume occurs at a pace and areal extent depending on the magnitude of the diversion (Figure 4). Salinity in Lake Pontchartrain is always low enough (< 15 PSU) to not limit N-fixing *Anabaena* sp. In 2011, salinity remained below 2 PSU on August 10th, indicating that salinity did not likely limit *Microcystis* sp. either. Salinity increased above 2 PSU following nitrate collapse in 2008 (Bargu et al., 2011; Figure 4), however at this time *Microcystis* sp. growth was likely restricted by lack of available DIN.

Our results illustrate a sequence of estuarine nutrient dynamics in response to large inflows of Mississippi River water (Figure 8): (1) high nutrient bioavailability in turbulent, sediment-rich conditions with a DIN:DIP molar ratio $\gg 16$, (2) rapid assimilation of DIP and NO₃⁻ during periods of increased light availability and reduced turbulence, (3) P-limitation of primary productivity, (4) nutrient-depleted conditions, and finally (5) a return to pre-inflow N-limitation following a rebound in DIP availability. Findings in 2008 (Bargu et al., 2011) and 2011 (this study) indicate that NO₃⁻ concentrations decrease rapidly to below detection in approximately

three weeks following spillway closure (Table 2). Only a small percentage of incoming NO_3^- is removed via denitrification in sediments (e.g., 3% in 2008) due to the immense NO_3^- loading rate during spillway openings (Roy et al., 2012). Therefore, the vast majority of loaded NO_3^- is either assimilated by phytoplankton or transported to the coastal ocean. The combination in 2011 of rapid NO_3^- decline and slow influx of higher salinity dilution water to the transect region (Figure 6) suggests that phytoplankton assimilation could possibly account for the majority of DIN-depletion that year. Further research is needed to make mass balance estimates of nitrate assimilated versus loaded to the coastal ocean. Nitrate remained the dominant form of DIN throughout the study period in 2011. Oscillations in $\text{NH}_4\text{-N}$ at low concentrations (Figure 6) were likely a result of mineralization processes, phytoplankton assimilation, and release from sediments due to concentration gradients (Wawrik et al., 2004; Roy et al., 2012).

Phosphorus bioavailability in Lake Pontchartrain during and after spillway events likely plays an important role in phytoplankton community response. The high DIN:DIP molar ratio of inflowing freshwater (≥ 50 , Table 2) leads to eventual P-limitation during the nitrate collapse period (Mize and Demcheck, 2009). Once loaded DIP is rapidly assimilated during this period, further primary production relies on internal sources of DIP including mineralization and internal loading from sediments. These P-limited conditions put N-fixing cyanobacteria (*Anabaena* sp.) at a competitive disadvantage (Paerl, 1988). Following the depletion of both water column DIP and DIN in 2011, the rapid rebound in DIP concentrations observed (Figure 6) could only occur by internal loading from sediments because northern tributaries were in drought conditions and there was no significant external source of DIP. Roy et al. (2012) show that internal P loading from Lake Pontchartrain sediments occurs regardless of bottom water oxygen availability and estimate that internal DIP loading by diffusion alone has the potential to regenerate water column DIP concentrations from below detection to the Mississippi River concentration during the 2011 event (0.05 mg P L^{-1}) in < 60 days. Our field observations (Figure 6) suggest that this internal pulse of P from sediments can return the system to pre-inflow N-limitation conditions even faster (< 1 month following spillway closure), perhaps due to additional advective flux. High Secchi disk transparency and low chlorophyll *a* measurements following July 11, 2011 (Figure 6) indicate that primary productivity was limited by N at this time. The dynamic interaction between high external N loading during inflows and subsequent internal P loading and return to N-limitation observed here (Figure 8) has rarely been documented in estuaries (Cook et al., 2010). Further research is needed to determine the impact of spillway openings on the potentially bioavailable phosphorus pool in Lake Pontchartrain sediments.

Si bioavailability is also a factor that can determine phytoplankton community response to inflows by influencing diatom success (Turner, 2002). The DSi:DIN molar ratio in Mississippi River water is near or above 1:1 during diversion periods (Table 2), indicating nutrient conditions favorable for diatom growth (Redfield et al., 1963; Officer and Ryther, 1980; Lane et al., 2001). Following nitrate collapse in 2011, DSi concentrations plummeted, potentially indicating diatom uptake, before rebounding a few weeks later (Figure 6). The observed rebound was likely due to the dissolution of diatom silica and resultant internal loading from sediments (Conley et al., 1988).

The Lake Pontchartrain environment is physically and chemically dynamic during and after spillway events, leading to dynamic biological response. The spatiotemporal dynamics of

cyanobacteria in 2008 illustrate a sequence of interrelated nutrient depletion and species appearance (Bargu et al., 2011). At stations directly influenced by the spillway plume, *Microcystis* sp. was the first cyanobacterium observed as NO_3^- depletion progressed (centric diatoms and chlorophytes were dominant), while *Anabaena* sp. was initially observed at low abundance in waters outside of the spillway plume influence where nutrient concentrations were low. Following depletion of spillway-loaded NO_3^- , there was a shift to cyanobacterial dominance by N-fixing *Anabaena* sp. It is likely that P release from sediments contributed to this bloom of N-fixers (Roy et al., 2012), as observed in other systems including the Baltic Sea (Vahtera et al., 2007). In contrast, cyanobacteria never achieved dominance following the 2011 closure (Figure 7).

The ecosystem dynamics in Lake Pontchartrain following freshwater inflow events that we have described (Figure 8) coupled with observations in 2008 lead to two questions about phytoplankton response in 2011. First, why wasn't there a bloom of *Microcystis* sp. immediately following the closure of the spillway when both DIN and DIP were readily available? Second, why wasn't there a bloom of N-fixing *Anabaena* sp. after spillway DIN was depleted, sediments provided an internal source of DIP, and N-limited conditions were restored?

There are two factors that may help answer the first question: water column physical disturbance and the form of DIN present. Surface water temperatures of 30°C likely enabled maximum growth rates for both chlorophytes and cyanobacteria upon spillway closure in 2011 (Paerl et al., 2011). The dominance of chlorophytes during the period of maximum phytoplankton biomass in 2011 (Figure 7), the absence of *Microcystis* sp. dominance in 2008, and previous observations of chlorophytes and diatoms outcompeting cyanobacteria during high inflow events in temperate estuaries (Paerl, 2006) all suggest that physical disturbance of the water column during spillway events may give chlorophytes or diatoms the competitive edge during the nutrient collapse period as light increases and horizontal displacement (i.e., flushing) continues. Whether diatoms or chlorophytes dominate is likely a function of temperature and therefore diversion timing, with higher temperatures similar to those observed in 2011 favoring chlorophytes. Another possible factor is the dominance of the DIN pool by NO_3^- . Blomqvist et al. (1994) suggest that high NO_3^- concentrations favor eukaryotic phytoplankton, while non-N-fixing cyanobacteria (*Microcystis* sp.) are more competitive at low NO_3^- concentrations with sufficient NH_4^+ . Observations by Jacoby et al. (2000) support this notion.

We hypothesize that the greater freshwater discharge, greater plume areal extent, and later diversion timing in 2011 compared to 2008 (Figures 2 and 3) all played important roles in limiting the success of N-fixing *Anabaena* sp. during the late summer period of N-limitation in 2011. The 2011 diversion occurred during the time period when CyanoHABs were observed in 2008 (Table 1). Hydraulic alteration to increase turbulence and flushing has been found to prevent or terminate *Anabaena* sp. blooms in river systems (Mitrovic et al., 2011). The spillway diversion may have essentially achieved the same function on a massive scale in Lake Pontchartrain in 2011, eliminating the *Anabaena* sp. seed population necessary for bloom formation.

The variability in Lake Pontchartrain ecosystem response to Bonnet Carré Spillway openings suggests that there is not a simple stimulus-response relationship between N loading and

estuarine CyanoHAB formation during large freshwater inflows. Nutrient loading during spillway openings consistently produces relatively high chlorophyll levels, however dominance of the phytoplankton community by CyanoHAB species is not guaranteed. A complex set of parameters including N loading, timing, diversion magnitude, plume hydrodynamics, nutrient molar ratios, internal P loading, weather, and northern tributary discharge can all play a role in ecosystem response. Our work provides a framework for understanding the relationships among large inflows of nitrate-rich freshwater to estuaries, internal nutrient dynamics, and factors determining cyanobacteria success (Figure 9). Physical disturbance of the water column associated with plume hydrodynamics and NO_3^- dominance of the DIN pool likely favor nonharmful phytoplankton species over non-N-fixing cyanobacteria during spillway openings and immediately following spillway closure when loaded nutrients are rapidly assimilated. Our results suggest that the magnitude and timing of hydraulic flushing in 2011 may have been responsible for the paucity of N-fixing cyanobacteria observed.

2012 Field Sampling

Nutrient Dynamics

Field data collected in 2012 indicates that northern tributaries to Lake Pontchartrain are a source of DIP and DIN during spring and summer (Figures 10 and 11). Mean DIP concentrations over the entire sampling period for Pass Manchac, the Tangipahoa River, and the Tchefuncte River were 0.065, 0.047, and 0.089 mg P L⁻¹, respectively. Mean DIN concentrations over the entire sampling period for Pass Manchac, the Tangipahoa River, and the Tchefuncte River were 0.046, 0.108, and 0.113 mg P L⁻¹, respectively. The DIN:DIP molar ratio at tributary sites varied between 0.9 and 12.3, always below the Redfield Ratio of 16, indicating that primary production in tributary waters was N-limited (Figure 12). Nutrient data collected in Lake Pontchartrain indicates that received DIN is rapidly assimilated resulting in DIN measurements rarely above the detection limit of 0.036 mg N L⁻¹ (Figure 11) and creating conditions where N-limitation of primary productivity persists at the both the transect stations and northwest corner stations throughout the spring and summer (Figure 12). At these times, DIP is available (Figure 10), most likely due to continued internal loading of P from sediments (Roy et al. 2012, Roy et al. 2013). These conditions are identical to conditions in Lake Pontchartrain prior to the spillway opening in 2011 and correspond to the state described in the upper left-hand corner of Figure 9 where N-limitation and available P favors N-fixing cyanobacteria.

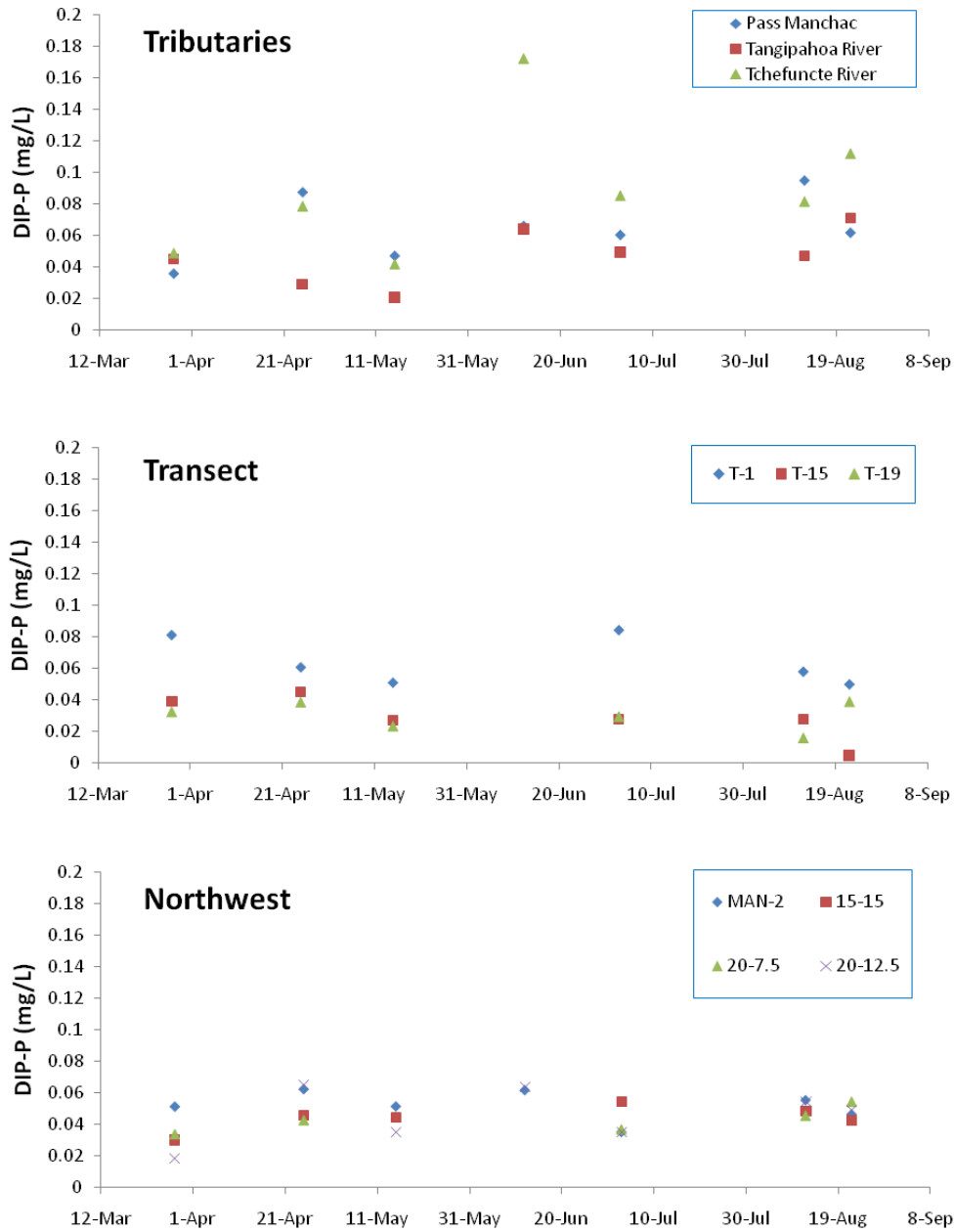


Figure 10. Dissolved inorganic phosphorus (DIP) concentrations in 2012 at tributary, transect, and northwest stations.

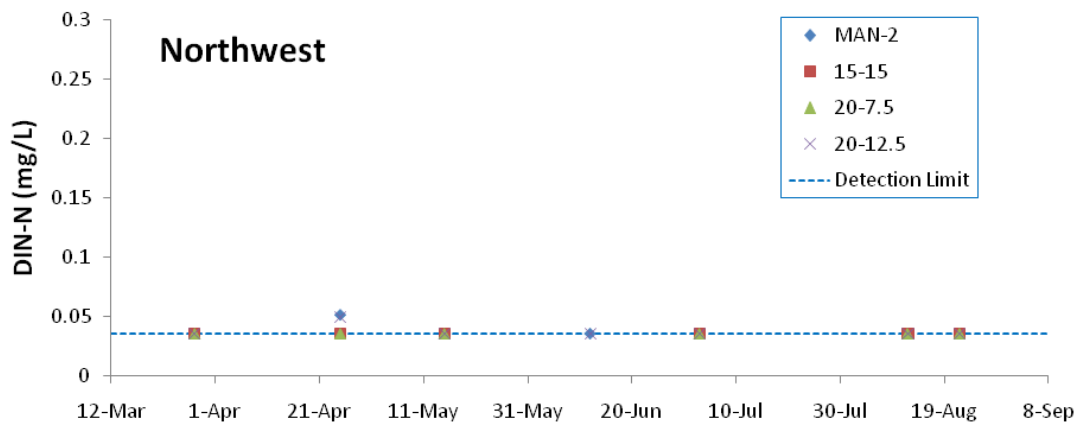
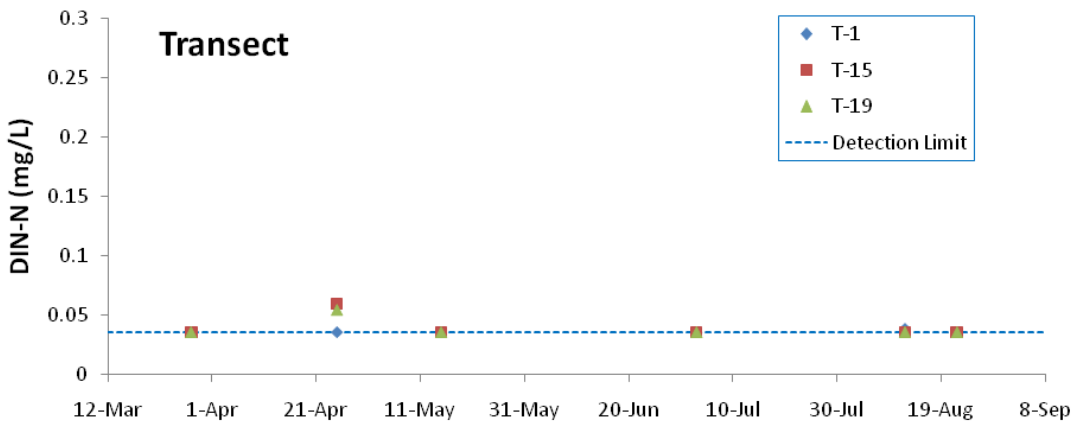
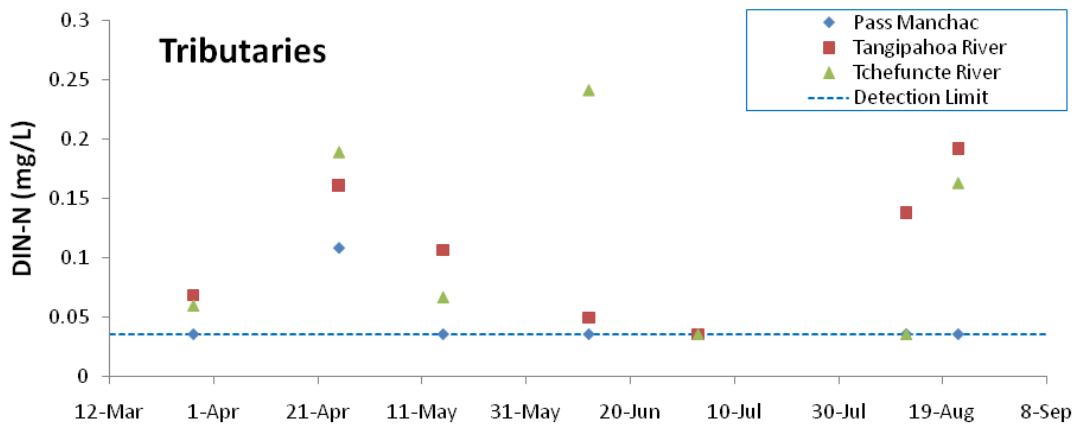


Figure 11. Dissolved inorganic nitrogen (DIN) concentrations in 2012 at tributary, transect, and northwest stations. Detection limit is 0.036 mg N L⁻¹.

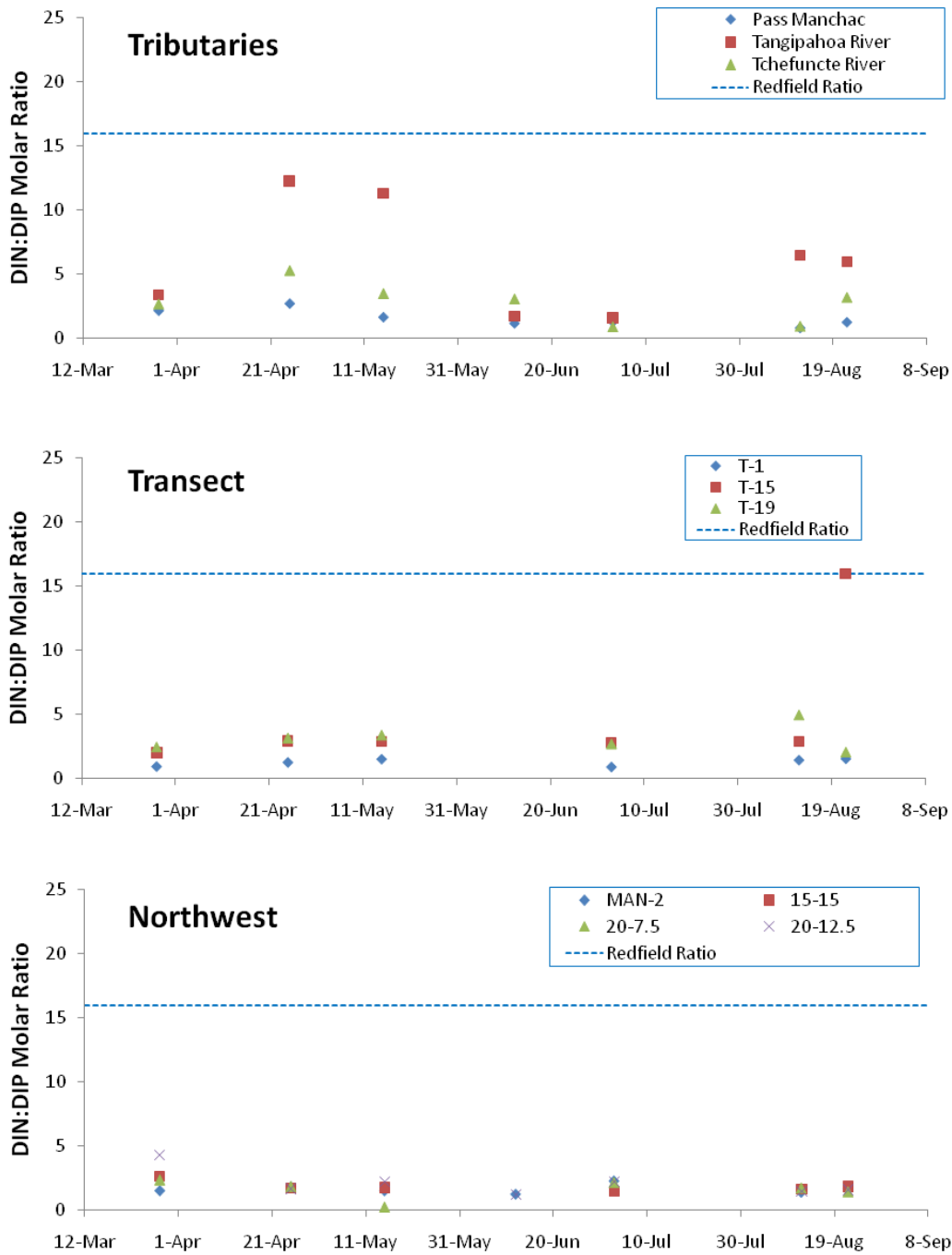


Figure 12. DIN:DIP molar ratios in 2012 at tributary, transect, and northwest stations. The Redfield Ratio (16) is shown. DIN:DIP > 16 indicates P limitation of primary productivity, whereas DIN:DIP < 16 indicates N limitation of primary productivity.

References

- Bargu S, White JR, Li C, Czubakowski J, Fulweiler RW. Effects of freshwater input on nutrient loading, phytoplankton biomass, and cyanotoxin production in an oligohaline estuarine lake. *Hydrobiologia* 2011;661:377-389.
- Conley DJ, Quigley MA, Schelske CL. Silica and phosphorus flux from sediments: importance of internal recycling in Lake Michigan. *Can. J. Fish. Aquat. Sci.* 1988;45:1030-1035.
- Cook PLM., Holland DP, Longmore AR. Effect of a flood event on the dynamics of phytoplankton and biogeochemistry in a large temperate Australian lagoon. *Limnol. Oceanogr.* 2010;55:1123-1133.
- Dortch, Q. & S. Achee, 1998. Lake Pontchartrain 1997 algal bloom: Identification, toxicity, and similar occurrences elsewhere in Louisiana coastal waters. In Malek-Wiley, R. R. (ed), *Clean Enough?* New Orleans: Lake Pontchartrain Basin Foundation: 19–20.
- Jacoby JM, Collier DC, Welch EB, Hardy J, Crayton M. Environmental factors associated with a toxic bloom of *Microcystis aeruginosa*. *Can. J. Fish. Aquat. Sci.* 2000;57:231-240.
- Lane RR, Day JW, Kemp GP, Demcheck DK. The 1994 experimental opening of the Bonnet Carre Spillway to divert Mississippi River water into Lake Pontchartrain, Louisiana. *Ecol. Eng.* 2001;17:411-422.
- Mize SV, Demcheck DK. Water quality and phytoplankton communities in Lake Pontchartrain during and after the Bonnet Carré Spillway Opening, April to October 2008, in Louisiana, USA. *Geo-Marine Letters* 2009;29:431-440.
- Officer CB, Ryther JH. The possible importance of silicon in marine eutrophication. *Mar. Ecol. Prog. Ser.* 1980;3:83-91.
- Paerl HW, Millie DF. Physiological ecology of toxic cyanobacteria. *Phycologia* 1996;35:160-167.
- Paerl HW, Hall NS, Calandrino ES. Controlling harmful cyanobacterial blooms in a world experiencing anthropogenic and climatic-induced change. *Sci. Total Environ.* 2011;409:1739-1745.
- Parsons T, Maita Y, Lali C. *A manual of chemical and biological methods for seawater analysis.* Oxford, UK: Pergamon Press;1984.
- Redfield AC, Ketchum BH, Richards FA. The influence of organisms on the composition of seawater. In: Hill MN, editor. *The sea*. Vol. 2. New York: John Wiley; 1963. p. 26-77.
- Roy ED, White JR, Smith EA, Bargu S, Li C. Estuarine ecosystem response to three large-scale Mississippi River flood diversion events. *Science of the Total Environment* 2013;458-460:374-387.
- Roy ED, Nguyen NT, Bargu S, White JR. Internal loading of phosphorus from sediments of Lake Pontchartrain (Louisiana, USA) with implications for eutrophication. *Hydrobiologia* 2012;684:69-82.
- Turner RE. Element ratios and aquatic food webs. *Estuaries* 2002;25:694-703.
- Turner RE, Dortch Q, Rabalais NN. Inorganic nitrogen transformations at high loading rates in an oligohaline estuary. *Biogeochemistry* 2004;68:411-422.
- USEPA (United States Environmental Protection Agency). *Methods of chemical analysis of water and wastes, USEPA 600/R-93/100.* Cincinnati: Environmental Monitoring Support Laboratory; 1993.

- Vahtera E, Conley DJ, Gustafsson BG, Kuosa H, Pitkänen H, Savchuk OP, Tamminen T, Viitasalo M, Voss M, Wasmund N, Wulff F. Internal ecosystem feedbacks enhance nitrogen-fixing cyanobacteria blooms and complicate management in the Baltic Sea. *Ambio* 2007;36:186-194.
- Wawrik B, Paul JH, Bronk DA, John D, Gray M. High rates of ammonium recycling drive phytoplankton productivity in the offshore Mississippi River plume. *Aquat. Microb. Ecol.* 2004;35:175-184.
- White JR, Fulweiler RW, Li CY, Bargu S, Walker ND, Twilley RR, Green SE. Mississippi River flood of 2008: Observations of a large freshwater diversion on physical, chemical, and biological characteristics of a shallow estuarine lake. *Environ. Sci. Technol.* 2009;43:5599-5604.

6. Student Support

Supported field and laboratory operations for Eric Roy and Emily Smith, Ph.D. students. In addition, this project funded two undergraduate student researchers.

Identification of contaminant source locations in Amite River watershed

Basic Information

Title:	Identification of contaminant source locations in Amite River watershed
Project Number:	2012LA84B
Start Date:	3/1/2012
End Date:	2/28/2012
Funding Source:	104B
Congressional District:	6th
Research Category:	Water Quality
Focus Category:	Models, Non Point Pollution, Solute Transport
Descriptors:	
Principal Investigators:	Zhi-Qiang Deng

Publications

1. Tong, Y. and Deng, Z. (2013). "Moment-Based Method for Identification of Pollution Source in Rivers." ASCE Journal of Environmental Engineering, DOI: 10.1061/(ASCE)EE.1943-7870.0000683 (in press).
2. Ghimire, B. and Deng, Z.-Q. (2013) "Hydrograph-based approach to modeling bacterial fate and transport in rivers." Water Research, 47 (3), 1329 – 1343, DOI: 10.1016/j.watres.2012.11.051.

Problem and Research Objectives

The Federal Clean Water Act (CWA) has played a major role in resolving point source pollution problems through a system of laws, regulations and judicial enforcement. However, pollutants from watershed-wide nonpoint sources are difficult to monitor and nearly impossible to regulate through the conventional CWA-based approach alone, often producing unknown source pollution to water bodies. In fact, the Louisiana's 2010 Integrated Report for water quality assessment indicated that about 82% of lakes and 16.6% of rivers in Louisiana are impaired by unknown sources, making it challenging to restore the impaired water bodies. The unknown source pollution may also be caused by illegal dumping or discharges. Therefore, the identification of pollution source location is essential to the restoration of water quality and thereby to the compliance with the CWA.

The overall goal of this project is to develop new methods for identifying the location of pollution sources, including both point and nonpoint sources. The proposed strategy is to test and demonstrate the new methods by identifying the locations of unknown pollution sources of BOD (Biochemical Oxygen Demand) in the Lower Amite River watershed (Figure 1). The Amite River, particularly the lower reach of Amite River, is impaired by BOD. Primary objectives of the project are: (1) to provide a simple yet effective method for identification of point contaminant source discharging to a river and (2) to develop a new method for identification of critical source areas of nonpoint source pollution in the Amite River watershed.

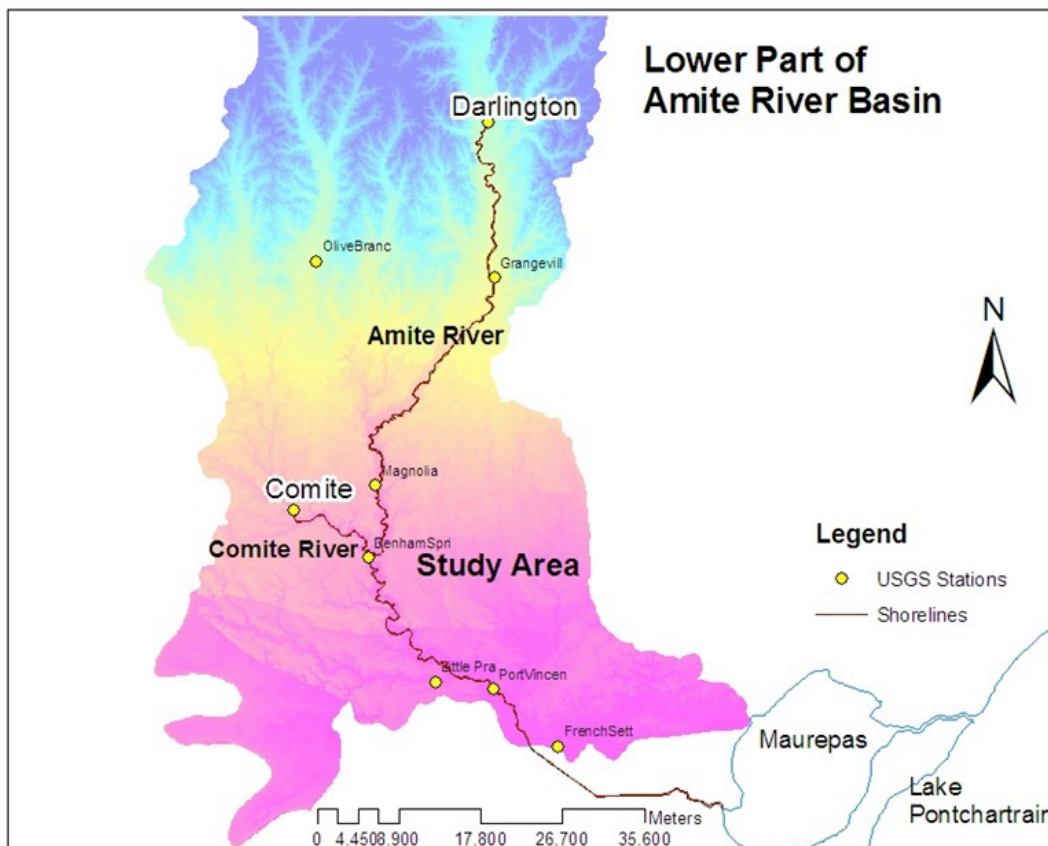


Figure 1. Map for the Amite River watershed.

Methodology

The objectives are accomplished by executing three tasks: (1) development of a moment-based method for identification of point pollution source by determining the location and total mass of discharge, (2) mapping watershed time of concentration by using US EPA program BASINS and watershed modeling tool HSPF; and (3) development of a watershed-based method for identification of nonpoint pollution source by locating unknown nonpoint source areas of BOD in the Amite River watershed. The proposed tasks are implemented by combining PI's proven variable residence time model for solute transport in rivers, watershed modeling systems BASINS/HSPF, and various data.

The project has broader implications for environmental restoration and sustainability in Louisiana and in the nation as well. This project provides an efficient and cost effective tool for environmental and water resources management agencies to locate unknown pollution sources from both point and distributed discharges and thus to reduce the uncertainty in TMDL development and implementation. While this study focused on the Amite River watershed, the approach developed in this study can be easily extended to other watersheds in Louisiana and in the nation. In addition, the project provided research and educational training opportunities for graduate and undergraduate students.

PRINCIPAL FINDINGS AND SIGNIFICANCE

1. Moment-Based Method for Identification of Pollution Source in Rivers (Paper 1)

- (1) A moment-based method is developed for identification of source location and quantity of accidental pollution along a river. The first two moment equations are derived through the Laplace transform of the Variable Residence Time (VART) model. While the first moment in combination with observed data is used to determine the location of pollution source (x), the second moment in combination with observed data is employed to estimate the total mass (quantity) of released pollutant (M_{est}). The two moment equations are written as:

$$x = \frac{\sum_{t=0}^{\infty} Ct}{\sum_{t=0}^{\infty} C} \sqrt{U^2 + 4K_s \frac{4\pi D_s}{A}} - \frac{2K_s}{\sqrt{U^2 + 4K_s \frac{4\pi D_s}{A}}} \quad (1)$$

$$M_{est} = Q \sum C(t_i) \Delta t_i \times (1 - CF), \quad i = 1, 2, \dots, n \quad (2)$$

where $CF(\%) = -0.4512 * [1 - \exp(-0.00939 \times \text{distance})]$ represents a distance correction factor (%) for the estimated total mass M_{est} ; x stands for the distance from the unknown pollution source location to the sampling station where concentration C and time t are recorded; U = cross-sectionally averaged flow velocity; K_s = longitudinal Fickian

dispersion coefficient; A = cross-sectional flow area of main channel; D_s = effective diffusion coefficient [L^2/T] in the storage zone; and Q is the river discharge.

- (2) The two moment equations are tested using 23 sets of conservative tracer injection data collected from 23 reaches in five rivers with the reach length ranging from about 3 km to 300 km. Results show that the first moment equation is able to predict the pollution source location with a percent error less than 18% in general (Figure 2). The percent error involved in the estimation of the corrected total mass is commonly less than 20% (Figure 3). While developed and tested using conservative tracer data, the moment-based method can also be applied to tracking the source location of reactive pollutants, providing a simple yet effective tool for pollution control and environmental management. The model predicted source location and mass (quantity) are compared with corresponding measured data in Figures 2 and 3, respectively.

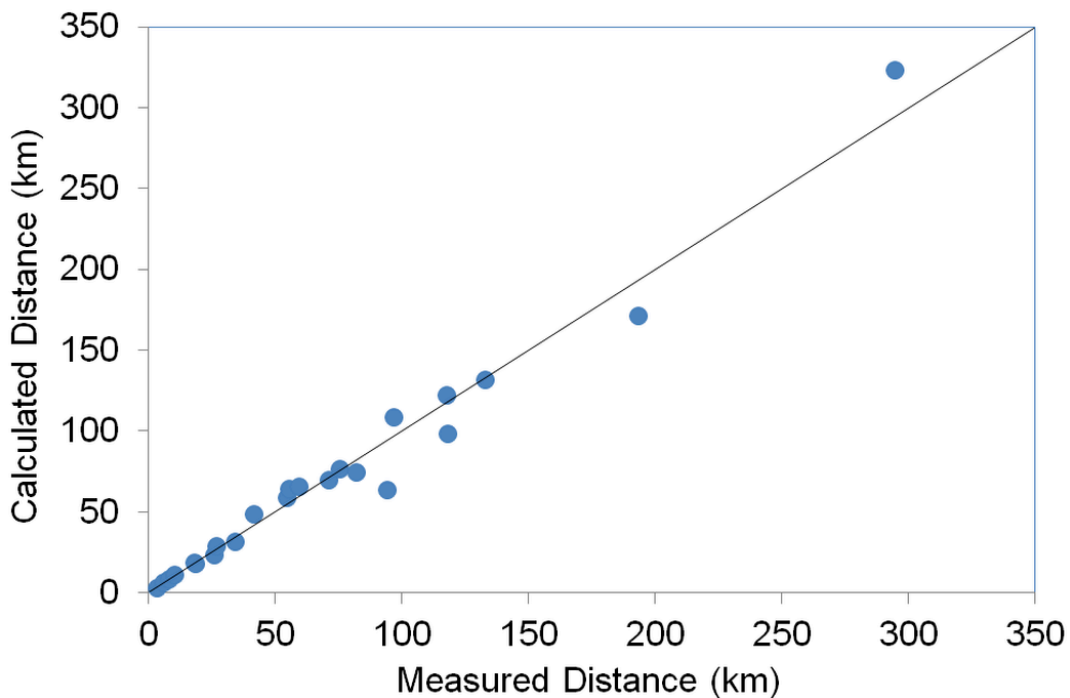


Figure 2. Comparison between calculated and measured distance.

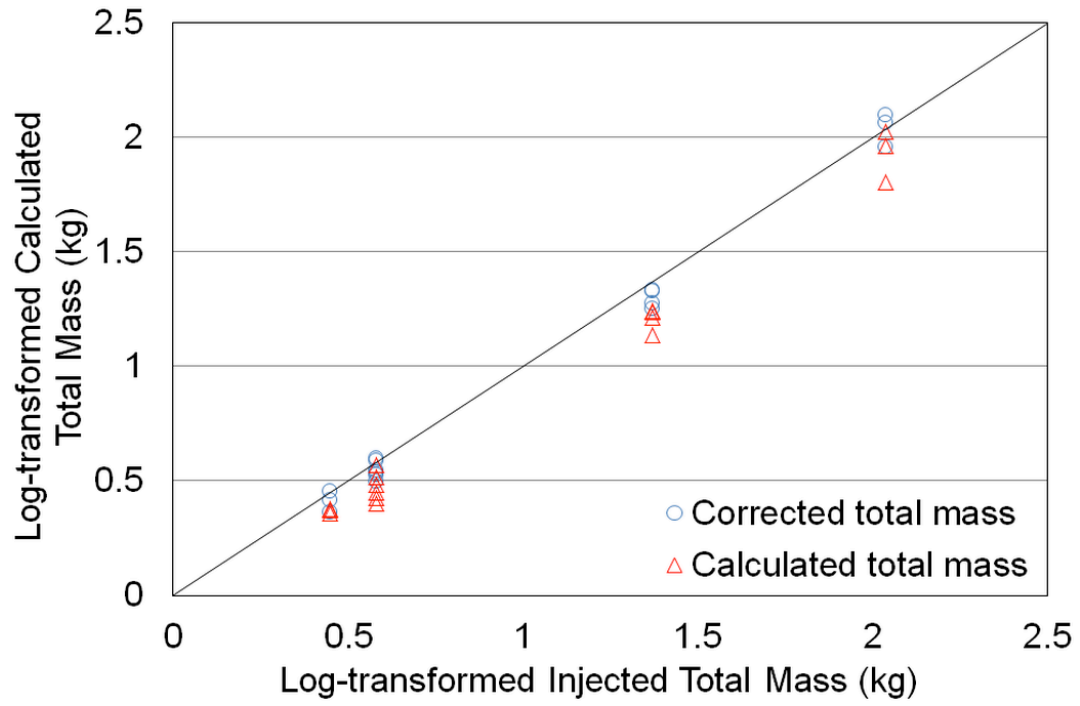


Figure 3. Comparison between calculated total masses with/without correction against injected total mass.

2. Identification of Critical Source Areas of Nonpoint Source Pollution (Paper 2)

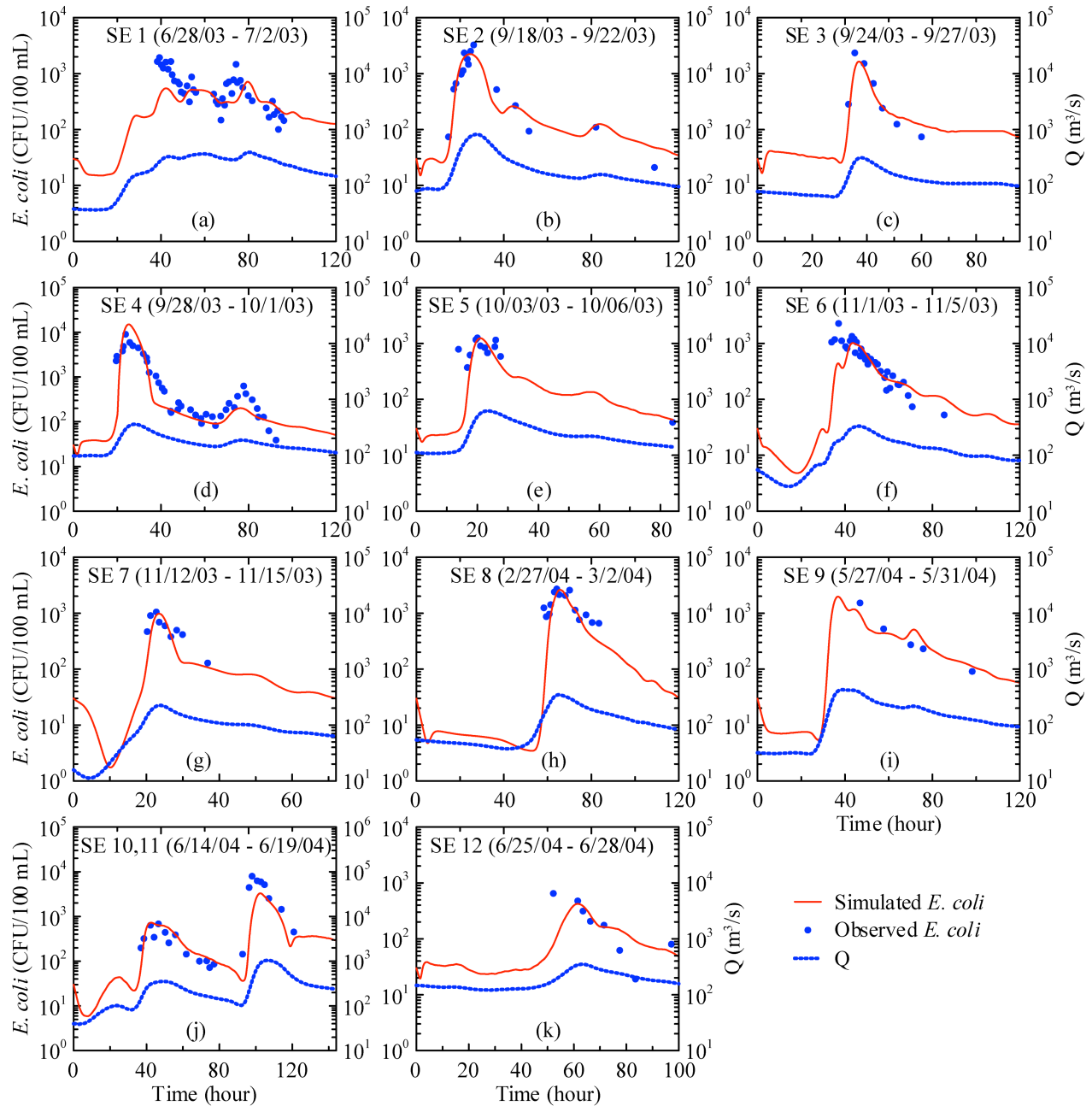


Figure 4. *E. coli* concentrations observed and simulated with the hydrograph-based approach.

- (1) A new hydrograph-based approach is proposed for predicting bacterial source and concentrations in rivers. Sediment resuspension from streambed may be an important source for bacterial transport during high flows. Results from this study indicate that the most important source responsible for bacterial transport in streams is watershed loading during flood events and hyporheic exchange during low flow periods. Figure 4 shows a

comparison between the observed and model predicted E. coli concentrations using the new hydrograph-based approach.

- (2) More details about the hydrograph-based approach to source area identification can be found in Paper 2.

3. Identification of Nonpoint Source Areas of BOD in Amite River Watershed

- (1) The variation in dissolved oxygen (DO) along the Amite River due to BOD loading from the watershed is mapped using ArcGIS and Google Earth to better understand the longitudinal variation in DO. The Google Earth map indicates that the DO level drops significantly downstream of the Claycut Bayou confluence and particularly the Bayou Manchac confluence, as shown in Figure 5, implying that the Claycut Bayou watershed and the Bayou Manchac watershed (Figure 6) are potentially the major source areas of DO pollution to the Lower Amite River. The Claycut Bayou and the Bayou Manchac collect runoff from the Baton Rouge metropolitan area.

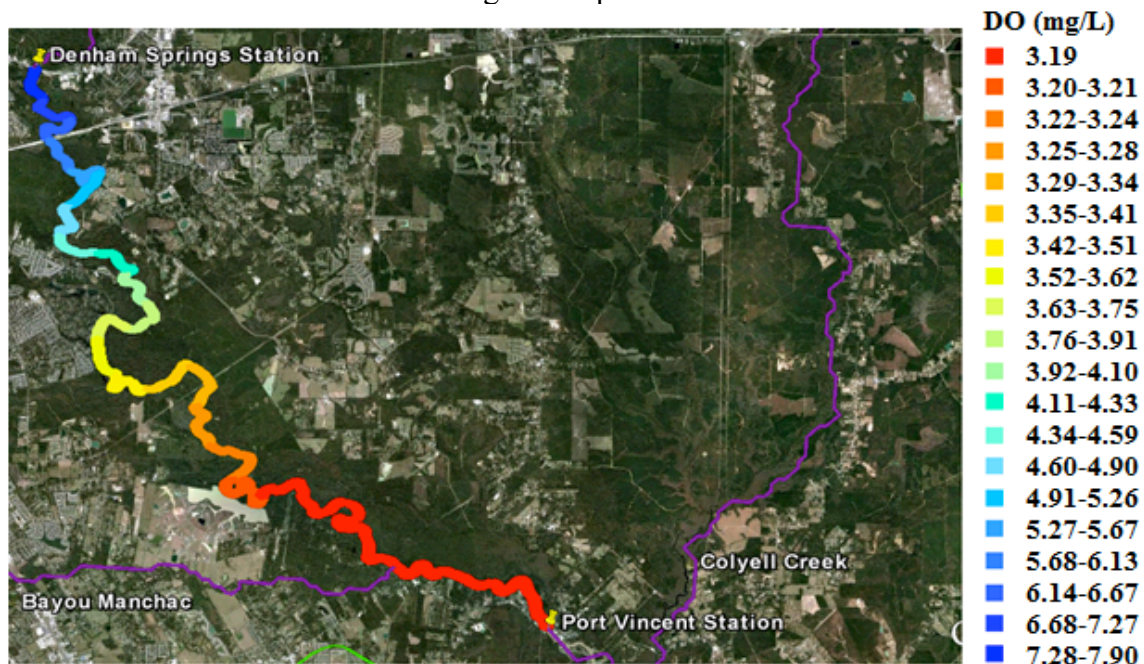


Figure 5. Reach-scale map showing DO variation along Amite River due to BOD loading from the watershed.

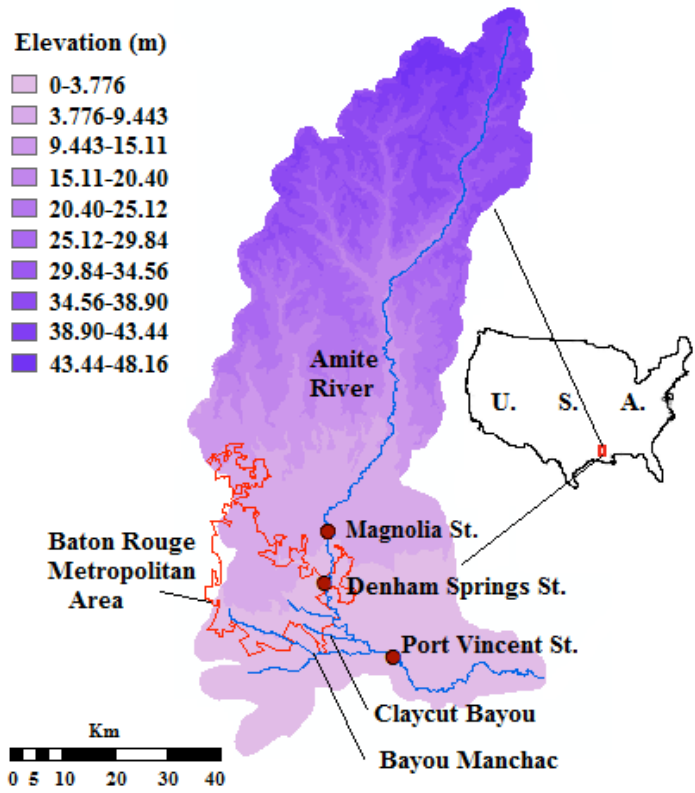


Figure 6. Map of Amite River watershed showing the critical source areas of BOD in the Claycut Bayou and the Bayou Manchac subwatersheds.

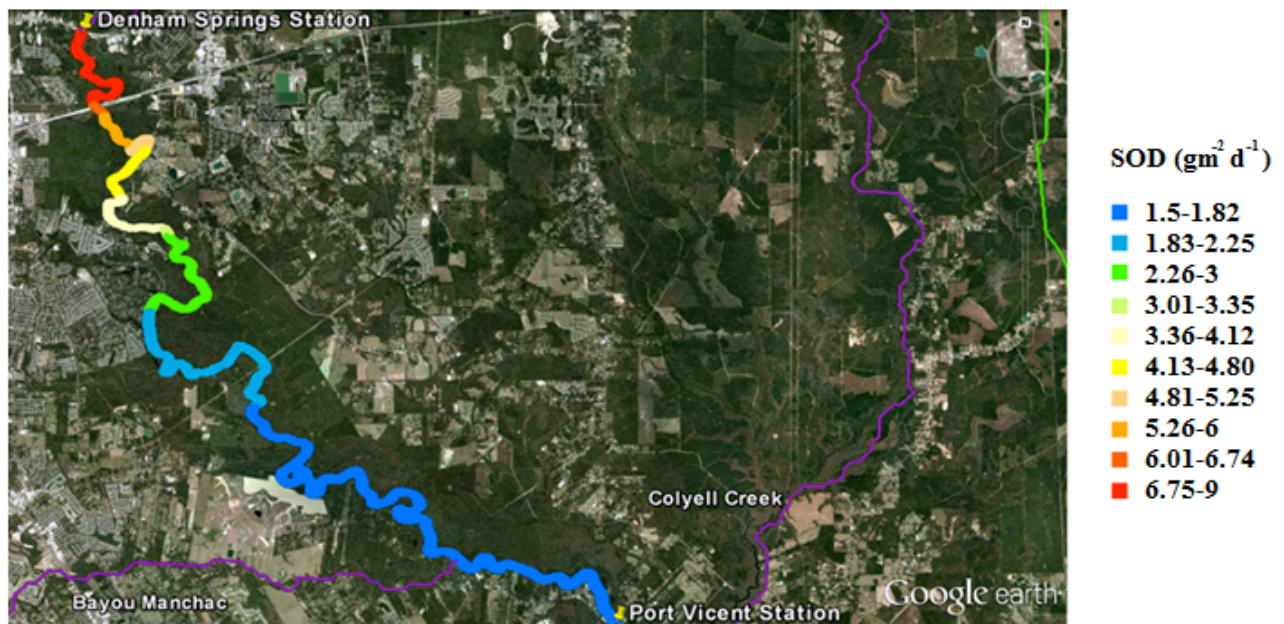


Figure 7. Spatial variation in SOD along Amite River between Denham Springs and Port Vincent Stations due to BOD loading from the watershed.

- (2) Figure 7 shows longitudinal variation in SOD along the 40 km-long Lower Amite River. The SOD is dependent on availability of DO in water column. The low SOD in the lower portion of the river reach is attributed to the low DO fluxes into the sediment layers due to low DO gradient across the sediment water interface. The SOD map in Figure 7 is consistent with the DO map in Figure 5, indicating again that the Claycut Bayou watershed and the Bayou Manchac watershed are the major source areas of DO pollution to the Lower Amite River. TMDL implementation efforts for the Amite River should focus on the restoration of the Claycut Bayou watershed and the Bayou Manchac watershed by implementing low impact development practices.

INFORMATION TRANSFER

The findings and methods developed in this project for identification of contaminant source locations in the Amite River Watershed will be transferred to the Louisiana Department of Environmental Quality for pollutant TMDL development and implementation and thereby for the restoration of the Lower Amite River.

STUDENT SUPPORT

Name of supported graduate student: Yangbin Tong (Male)

Degree Program: M.S. in Water Resources

Thesis Title: Development of Watershed-Based Modeling Approach to Critical Source Area Identification

Graduation Date: August 2013

Name of supported graduate student: Bhuban Ghimire (Male)

Degree Program: Ph.D. in Water Resources

Dissertation Title: Development of Hydrograph-Based Approach to Modeling Fate and Transport of Sediment-Borne Bacteria in Lowland Rivers

Graduation Date: May 2012

Name of supported undergraduate student: Julian Moore (Male)

Degree Program: B.S. in Environmental Engineering

Research Topic: EVEG 3273 Independent Research

Graduation Date: December 2012

FOLLOW-ON FUNDING

Proposal Title: **Process-Based Modeling and Mitigation of Nitrogen and Phosphorus Inputs in Boeuf River Watershed (in review)**

PI: Zhiqiang Deng

Funding Agency: USDA (National Institute of Food and Agriculture)

Hydrostratigraphy Modeling of the Southern Hills Aquifer System and Faults

Basic Information

Title:	Hydrostratigraphy Modeling of the Southern Hills Aquifer System and Faults
Project Number:	2012LA85B
Start Date:	3/1/2012
End Date:	2/28/2012
Funding Source:	104B
Congressional District:	6th
Research Category:	Ground-water Flow and Transport
Focus Category:	Groundwater, Solute Transport, Methods
Descriptors:	
Principal Investigators:	Frank Tsai

Publications

1. Elshall, A. S., F. T.-C. Tsai, J. S. Hanor, Indicator geostatistics for reconstructing Baton Rouge aquifer-fault hydrostratigraphy (Louisiana, USA), *Hydrogeology Journal*, 2013. (accepted)
2. Tsai, F. T.-C. and A. S. Elshall, Hierarchical Bayesian model averaging for hydrostratigraphic modeling: Uncertainty segregation and comparative evaluation, *Water Resources Research*, 2013. (accepted)
3. Frank Tsai and Jeffrey Hanor, 2012, Hierarchical Multimodel Saltwater Intrusion Remediation and Sampling Designs: A BMA Tree Approach, Louisiana Water Resources Research Institute, Louisiana State University, Baton Rouge, Louisiana, 10 pages. (USGS 104G)
4. Frank Tsai, 2012, Feasibility Study of Scavenging Approach to Stop Saltwater Toward Water Wells, Louisiana Water Resources Research Institute, Louisiana State University, Baton Rouge, Louisiana, 10 pages. (USGS 104B)
5. Tsai F. T.-C. Tsai, and A. S. Elshall, A Bayesian Model Averaging Method to Characterize the Baton Rouge Aquifer System, 2012 World Environmental & Water Resources Congress, Albuquerque, NM, May 20-24, 2012
6. Beigi, E., and F. T.-C. Tsai, Climate Impact on Groundwater Recharge in Southeastern Louisiana and Southwestern Mississippi, H13B-1317 Abstract, 2012 American Geophysical Union Fall Meeting, San Francisco, CA, 3-7 December 2012
7. Elshall, A. S., F. T.-C. Tsai, J. S. Hanor, Hydrogeophysical Data Fusion and Geostatistical Approach to Characterize Hydrogeological Structure of the Baton Rouge Aquifer System in Louisiana, H13B-1336 Abstract, 2012 American Geophysical Union Fall Meeting, San Francisco, CA, 3-7 December 2012
8. Pham, H. V., A. S. Elshall, F. T.-C. Tsai, and L. Yan, Local Derivative-Free Parallel Computing Method for Solving the Inverse Problem in Groundwater Modeling, H21A-1164 Abstract, 2012 American Geophysical Union Fall Meeting, San Francisco, CA, 3-7 December 2012
9. Chitsazan, N. and F. T.-C. Tsai, Hierarchical Bayesian Model Averaging for Chance Constrained Remediation Designs, H33I-1450 Abstract, 2012 American Geophysical Union Fall Meeting, San Francisco, CA, 3-7 December 2012
10. Tsai, F. T.-C., A. S. Elshall and J. S. Hanor, A Hierarchical Multi-Model Approach for Uncertainty Segregation, Prioritization and Comparative Evaluation of Competing Modeling Propositions, H43B-1326 Abstract, 2012 American Geophysical Union Fall Meeting, San Francisco, CA, 3-7

Hydrostratigraphy Modeling of the Southern Hills Aquifer System and Faults

December 2012

Problem and Research Objectives

The Southern Hills aquifer system shown in Figure 1(a) was designated to be the sole source aquifer for southeastern Louisiana and southwestern Mississippi (Buono 1983; USEPA Region 4 & 6). The Southern Hills aquifer system also provides an essential amount of high quality groundwater for industries in Louisiana. In 2000, 290 million gallons per day of groundwater were withdrawn from the Southern Hills aquifer system, of which 49% were used for public supply and 39% were used for industries (Sargent 2002). Figure 1(b) shows the 2009 groundwater withdrawals by 33 public suppliers and industries in East Baton Rouge Parish. Due to excessive groundwater withdrawal, many freshwater sands in the Southern Hills aquifer system north of the Baton Rouge fault are being contaminated by saltwater intrusion from brackish aquifers south of the fault (Tomaszewski 1996; Lovelace 2009).

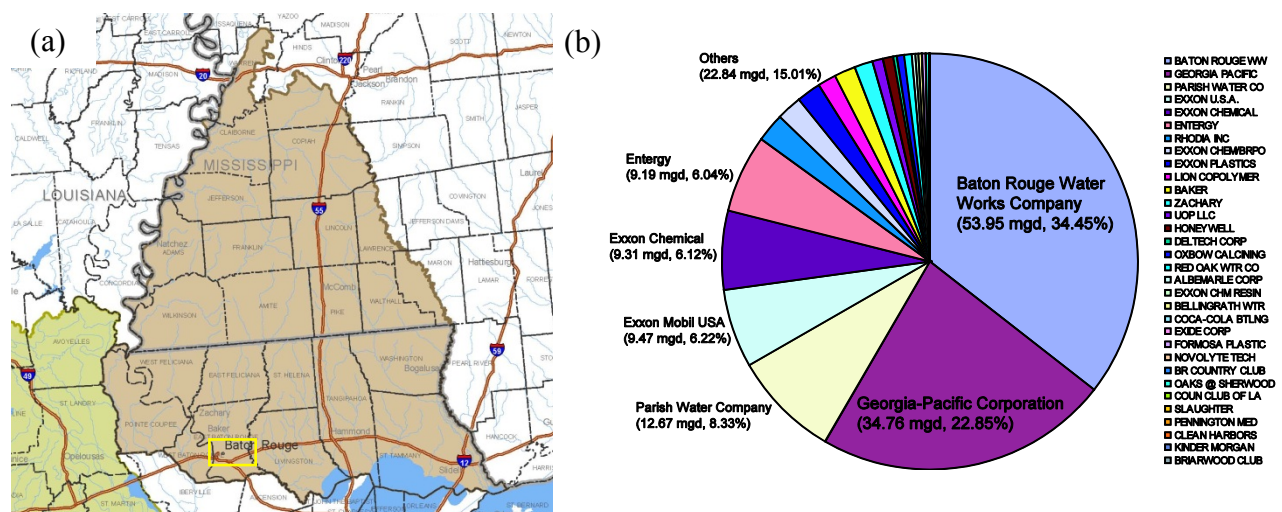
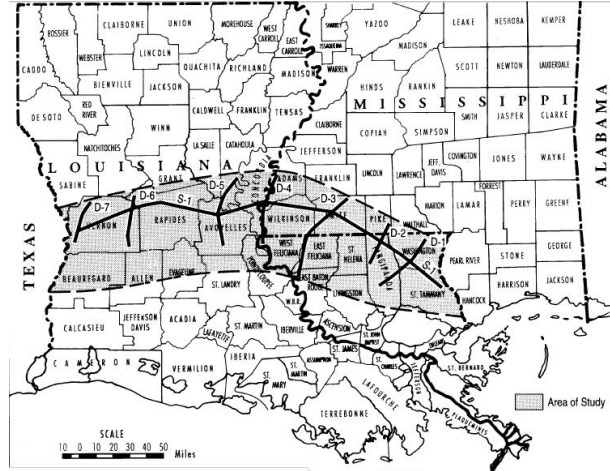


Fig. 1: (a) The Southern Hills aquifer system (map source: USEPA Region 6). The yellow box is the current study area under saltwater intrusion, shown. (b) 2009 groundwater withdrawals by 33 public suppliers and industries from the aquifers in East Baton Rouge Parish (data source: CAGWCC).

Saltwater intrusion, recent drought (based on the U.S. Drought Monitoring), climate change and concerns of groundwater shortage/contamination by natural gas shale fracking prompts the development of a “Statewide Groundwater Management Plan” by the Louisiana Department of Natural Resources (DNR) starting in 2010 (Ecology and Environment, Inc. 2010). This Plan is especially intriguing to citizens in the Southern Hills aquifer system after the oil and gas industries expressed a strong interest in developing the Tuscaloosa Marine Shale (Welsh 2011), which covers almost the entire Florida Parishes shown in Figure 2. Recently, the DNR issued “Recommendations for a Statewide Ground Water Management Plan” (Ecology and Environment, Inc. 2011) that “requests the legislature to develop a program to fund the development of aquifer-wide groundwater availability models...” The Recommendation recommended Louisiana GWMATF (Ground Water Management Advisory Task Force) to study and identify (1) type and frequency of modeling suggested per area; (2) initial and annual maintenance cost to implement suggested modeling projects per area; and (3) sustainable funding sources for each project.

Developing reliable *groundwater availability models* needs to understand the complexity of an aquifer system. The proposal aims to develop a geostatistical hydrostratigraphy technique to understand the complexity of the Southern Hills aquifer system. The technique can also be applied to other aquifer systems.

Fig. 2: Extent of Tuscaloosa Marine Shale (John et al. 1997)



The goal of the project is to construct detailed hydrostratigraphy of the Southern Hills aquifer system. The scope of the project includes collection of geophysical logs, driller logs and well schedules from the DNR, USGS, LGS and CAGWCC, interpretation of well logs into sand-clay binary hydrostratigraphy, calibration of three-dimensional hydrostratigraphy, and identification of faults in the aquifer system.

Objectives

To achieve the project goal, we propose the following specific objectives:

Objective 1 Delineate aquifer structure

The objective is to better understand hydraulic connection from outcrops to the south boundary of the Southern Hills aquifer system.

Objective 2 Delineate fault structure

The objective is to calculate displacement of aquifers across faults and identify flow pathways that saltwater crosses the Baton Rouge fault.

Methodology (from Elshall et al., 2013 Hydrogeology Journal)

1. Indicator generalization parameterization for hydrostratigraphy modeling

In this study, parameterization is conducted in the two-dimensional planar direction along the dip for every one-foot vertical interval. Three-dimensional aquifer-fault architecture is reconstructed by assembling all two-dimensional slices.

This study utilizes a generalized parameterization (GP) method (Tsai and Yeh 2004; Tsai 2006), which combines the indicator kriging (IK) and indicator zonation (IZ) through a set of data weighting coefficients to obtain nonsmooth conditional estimates. The indicator function $\{I(\mathbf{x}, \nu) : \mathbf{x} \in \text{study area}\}$ is a random function with the indicator random variable ν describing the spatial extent of sand or clay facies. For a given sand-clay cutoff α , the random function of the indicator random variable ν for sand facies is defined as

$$I(\mathbf{x}, \nu) = \begin{cases} 1 & \nu \in \text{Sand}, \nu(\mathbf{x}) \geq \alpha \\ 0 & \nu \notin \text{Sand}, \nu(\mathbf{x}) < \alpha \end{cases} \quad (1)$$

From equation (1) the indicator outcome (one or zero) indicates the presence of sand facies or clay facies, respectively. The indicator variogram has the same definition as the normal

variogram except that the real random function is replaced by the indicator random function $I(\mathbf{x}, v)$. To calculate the expected value $v^*(\mathbf{x}_0)$ at location \mathbf{x}_0 , the GP is

$$v^*(\mathbf{x}_0) = I(\mathbf{x}_k) + \sum_{i=1}^N \lambda_i [I(\mathbf{x}_i) - I(\mathbf{x}_k)] \beta_i \quad (2)$$

where N is the number of electric well logs, $I(\mathbf{x}_i)$ is the indicator data, λ_i is the indicator kriging weight, and β_i is the data weighting coefficient for a data point of a well log at location \mathbf{x}_i . $I(\mathbf{x}_k)$ is indicator data for a zone defined by well log k . Equation (2) shows that GP estimate at unknown location is similar to IK estimate $v^*(\mathbf{x}_0) = \sum_{i=1}^N \lambda_i I(\mathbf{x}_i)$ or the IZ estimate $v^*(\mathbf{x}_0) = I(\mathbf{x}_k)$ except for the introduction of β_i such that $\forall \beta_i = 1$ gives the IK estimate, $\forall \beta_i = 0$ gives the IZ estimate and $0 < \beta_i < 1$ gives the in-between GP estimate.

For zonal delineation, this study uses two-dimensional Voronoi tessellation (Sibson 1980). This is a simple mathematical technique for dividing a space into a number of Voronoi zones, given a set of coplanar points, which are electric well logs data. A Voronoi zone, which is drawn based on bi-sectors for each data point, is a boundary enclosing all the intermediate space lying nearest to that data point than to other data points in the plane. The Voronoi tessellation is considered a neutral and unbiased approach to define the neighborhood of a data point (Tsai and Yeh 2004; Tsai 2006).

2. Unknown model parameters

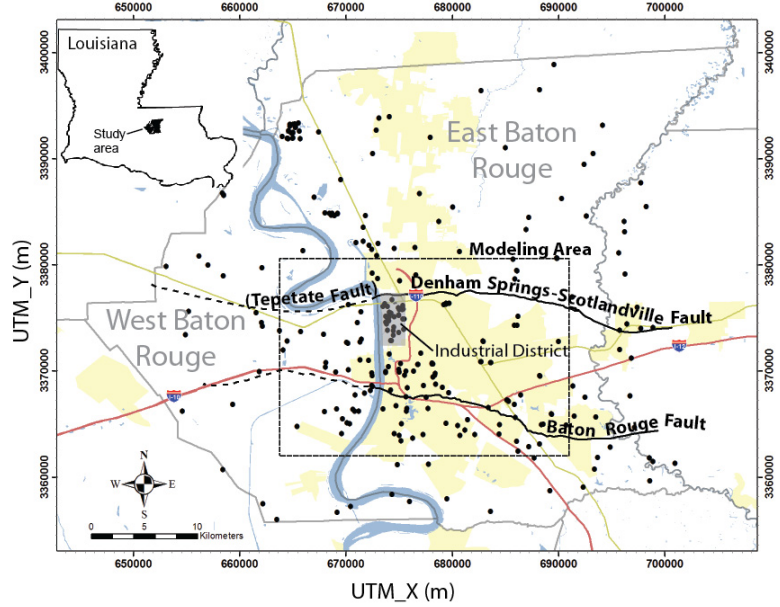
The first unknown model parameter is the formation dip, which establishes data correlation. The Baton Rouge aquifer system gently dips south. Prior geological studies did not quantify the formation dip. The dip was calculated to be $0.30^\circ \pm 0.06^\circ$ from the USGS cross-sectional maps in the area (Griffith 2003) as prior information. To constrain the search space, the dip is set within the range $0.06^\circ \leq \phi \leq 0.60^\circ$. The vertical tolerance of the dip is not reported in any study, and no vertical tolerance is considered.

The second unknown model parameter is the sand-clay cutoff value α . The estimated v values, which cutoff value rounds to produce an indicator, could be viewed as the conditional probability with respect to the binary variables (Chilès and Delfiner 1999). The limits of the cutoff value α are constrained to a realistic but flexible range of $0.3 \leq \alpha \leq 0.7$. Other unknown model parameters are the data weighting coefficients β of the well logs.

For reconstructing aquifer-fault architecture in the Baton Rouge area shown in Figure 3, the model used 288 geophysical well logs in which the south, middle and north domains have 61, 129 and 98 well logs, respectively, to reconstruct the hydrostratigraphy. When the spacing of well logs is dense, the estimates by the GP method in these areas become insensitive to the data weighting coefficients β , since the indicator kriging estimates and indicator zonation estimates are similar. To reduce the computational cost of the inverse problem, insensitive values of β are identified through sensitivity analysis. Performing the sensitivity analysis starts by calibrating the hydrostratigraphy model only with respect to the dip and cutoff for given $\forall \beta = 1$ to all well logs,

and then using the calibrated model as a reference for the fitting error. Then taking one well log at a time, its data weighting coefficient is evaluated from 0 to 1 incrementally by 0.1 to calculate new fitting errors. Any well log that results in an error difference less than $\pm 0.05\%$ from the calibrated model is considered to have a fixed data weighting coefficient $\beta = 1$. The sensitivity analysis shows that 48 well logs have sensitive β coefficients with their number in the south, middle and north domains being 6, 34 and 8 well logs, respectively.

Fig. 3. Map of the study area in the Universal Transverse Mercator (UTM) coordinate system. Black dots represent the location of electrical well logs. The bold solid lines are fault lines identified by the surface expression (McCulloh and Heinrich 2012). The bold dashed lines are the approximate surface locations of the faults (Griffith 2003). The yellow areas are urban areas, the grey lines are parish borders, the red lines are interstate freeways, the green lines are US highways, and the blue areas and lines are water bodies.



3. Inverse problem

The data weighting coefficients β along with the dip ϕ and sand-clay cutoff α are the unknown model parameters to be estimated using an inversion scheme. The inversion scheme for the IZ, IK and GP is the same except for the size of the unknown parameters. The IZ inversion has only one unknown parameter that is the dip. The unknown parameters of the IK inversion are the dip and the cutoff. The unknown parameters of the GP inversion are the dip, the cutoff and the data weighting coefficients. The inverse problem is formulated by minimizing the mean squared error between the estimated and observed facies as follows:

$$\min_{\phi, \alpha, \beta} \frac{1}{2} \left\{ \frac{1}{M_{sand}} \sum_{i=1}^{M_{sand}} [I^{i,est}(\mathbf{x}) - I_{sand}^{i,obs}(\mathbf{x})]^2 + \frac{1}{M_{clay}} \sum_{i=1}^{M_{clay}} [I^{i,est}(\mathbf{x}) - I_{clay}^{i,obs}(\mathbf{x})]^2 \right\} \quad (3)$$

where M_{sand} and M_{clay} are the number of data points of the sand facies and clay facies, respectively. The $I^{i,est}(\mathbf{x})$, $I_{sand}^{i,obs}(\mathbf{x})$ and $I_{clay}^{i,obs}(\mathbf{x})$ are the indicator estimate, the observed sand facies indicator and the observed clay facies indicator at a location \mathbf{x} , respectively. The mean squared error is separated into two error terms with one for each facies to avoid calibration bias toward favoring the fitting of clay over sand since the well logs indicate a clay proportion of about two-third by volume within the study area. The proportion of sand calculated from the electric logs is 0.338 and is 0.339 from the drillers' logs. This separation underlines that reducing the sand error is equally important as reducing the clay error.

To solve the inverse problem, the study adopts the Covariance Matrix Adaptation Evolution Strategy (CMA-ES) (Hansen et al. 2003) as a local derivative-free optimization method for two reasons. First, unlike the derivative-based methods, using the CMA-ES allows for flexible optimization without prior assumptions or restrictions about the model structure. Second, the enhanced search properties of the CMA-ES allow for reaching near global solution. Similar to other generation-based optimization algorithms, the CMA-ES proposes several candidate solutions per search iteration. Each candidate solution is a vector of unknown model parameters, which the model uses to solve for state variables. Then the objective functions of all solutions are calculated and ranked. The CMA-ES adapts a covariance matrix representing the pair-wise dependency between unknown model parameters, which approximates the inverse of the Hessian matrix up to a certain factor. The covariance matrix adaptation uses information from the ranking of the current solutions and from the previous search path. Then the solutions are updated with the covariance matrix and an adaptable step size, which are adapted through two conjugates that implements heuristic control terms. These enhanced search properties allow the CMA-ES to handle ill-conditioned, nonsmooth, discontinuous, nonconvex and multimodal functions. Reviewing the CMA-ES algorithm is beyond the scope of this work, and reader is referred to Hansen (2006) and the references therein.

The inversion scheme steps are as follows. First, the CMA-ES generates candidate solutions, which are sets of unknown model parameters. Second, for each proposed solution the experimental variograms and a theoretical variogram are calculated based on the proposed dip. With respect to experimental variograms it is important to clarify one precaution with respect to location dependence of data correlation is accounted for. The correlation between the data across the faults is prevented, but all the experimental variograms of each domain are grouped together to calculate one theoretical variogram. The theoretical variograms is fitted to the experimental variograms automatically through using the pattern search method. It performs direct directional search for the correlation parameters, which are the nugget, sill and effective range, to minimize the squared root error between the experimental and the theoretical variograms. Third, interpolation function in equation (2) is used to estimate facies distribution at unknown locations. For the inversion purpose the unknown locations are the drillers' logs locations. For the IZ inversion all the β values are set to zero, and thus the cutoff is not needed. Contrariwise, for the IK inversion the β values are set to one, thus the estimated facies is rounded to the indicator value by the cutoff. For the GP inversion β values are used by the interpolation function in equation (2) to estimate facies distribution at the unknown locations and the cutoff is used to round the indicator. Fourth, the estimated facies are compared to the observed facies to calculate the mean squared error for individual solutions. Then, step 1 is repeated until the mean squared error is minimized.

The outcome of the inversion is the best unknown model parameters set that fits the observed facies. This parameters set (dip, cutoff and β values) can be used to plot any 2-dimensional or 3-dimensional diagrams according to the desired grid size. For example, in this study all the cross sections of the faults have a grid size of 50 m along the fault lines. The 3-dimensional diagrams of the aquifer system have a grid size of 200 m in the X and Y directions. The discretization in Z direction is 1-foot (0.34-m) interval.

Principal Findings and Significance (from Elshall et al., 2013 Hydrogeology Journal)

1. Calibration results

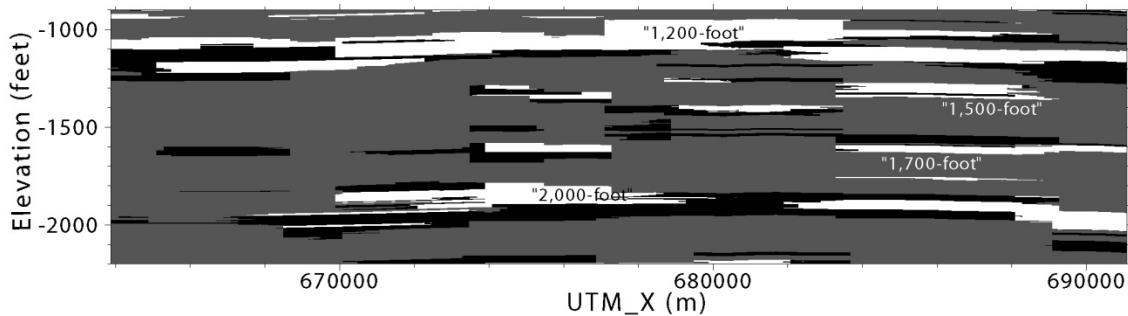
This inversion scheme is used to obtain the optimal data weighting coefficients, dip, and cutoff for the hydrostratigraphy model. The calibration results are shown in Table 1. The variogram structure and cutoff are similar for the indicator zonation (IK), generalized parameterization (GP), and indicator kriging (IZ) methods. The three methods also show the same dip around 0.29° and the same sand proportion around 0.35. The GP shows less fitting error than the IK and IZ methods due to the flexibility of the method.

Table 1. Estimated Variogram Structural Parameters and Model Parameters for the Three Methods.

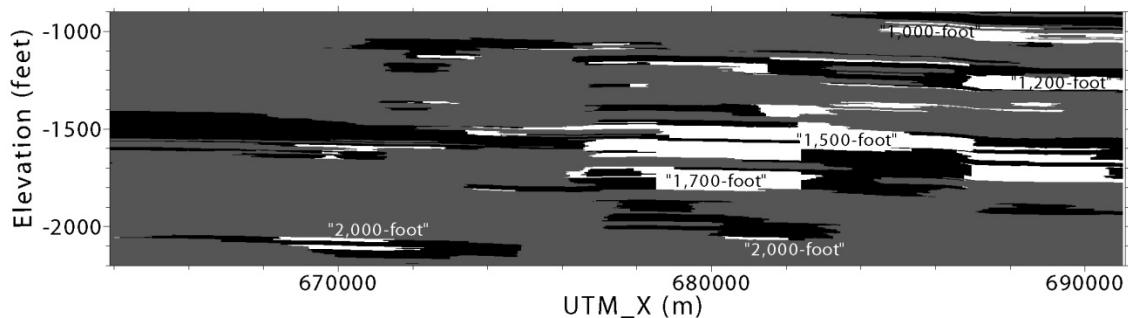
Method	Nugget	Sill	Range [m]	Dip [Deg.]	Cutoff [-]	Sand Proportion	Sand Error[%]	Clay Error[%]	Total Error[%]
IZ	0.062	0.161	8400	0.276	-	0.340	13.02	12.79	12.91
GP	0.083	0.139	8400	0.289	0.404	0.347	11.96	12.90	12.43
IK	0.084	0.139	8600	0.286	0.404	0.347	12.04	12.96	12.50

2. Fault architecture

To show the differences between the three methods, the architecture of the Denham Springs-Scotlandville fault and the Baton Rouge fault are used as examples. Figure 4 show the juxtaposition at the fault cross sections using the generalized parameterization method. Black areas are clay units north of the fault. Gray areas are clay units south of the fault. Sand units are transparent to show potential hydraulic connections through the fault. It is noted that the faults are three-dimensional zones of deformation, not two-dimensional planes. Determination of permeability of the fault zone is suggested by Bense and Person (2006) and Hanor et al. (2011). Nevertheless, the detailed architecture of the fault zone is not the scope of this study.



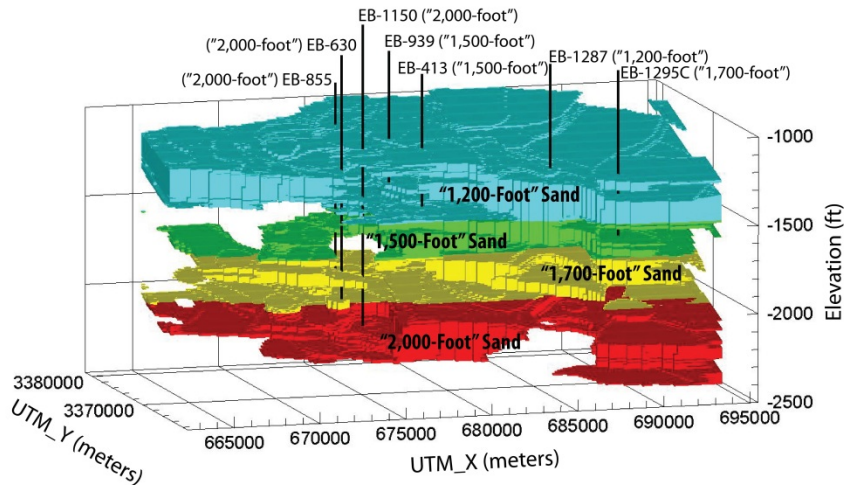
(a) Denham Springs-Scotlandville Fault



(b) Baton Rouge Fault

Fig. 4. (a) the architecture of the Denham Springs-Scotlandville fault in the modeling area using generalized parameterization, and (b) the architecture of the Baton Rouge fault in the modeling area using generalized parameterization. Black areas are clay units north of the fault. Gray areas are clay units south of the fault. Sand units are transparent to show potential hydraulic connections through the fault. The fault cross sections are based on 3D estimates that follow the UTM_X and UTM_Y coordinates of the fault line in Figure 3. Elevation is feet above NGVD29.

Fig. 5. Hydrostratigraphic architecture of the “1,200-foot” sand to the “2,000-foot” sand in the middle domain of the modeling area in Figure 3. The wells in the figure are public supply and industrial wells.



3. Aquifer architecture

Figure 5 shows the simulated aquifer architecture from the “1,200-foot” sand to the “2,000-foot” sand in the middle domain based on the GP method. The “1,200-foot” sand connects vertically to the “1,500-foot” sand. The “2,000-foot” sand is clearly separated from the “1,700-foot” sand by a confining layer. There are four sand units between the “1,200-foot” sand and the “2,000-foot” sand, which are generally classified as the “1,500-foot” sand and the “1,700-foot” sand (Griffith 2003). Unlike the distinguishable “1,200-foot” sand and the “2,000-foot” sand, the separation of the “1,500-foot” sand from the “1,700-foot” sand is not well-defined in the published cross sections (Rollo 1969; Griffith 2003). The findings of this study also show that they are not clearly separable. Therefore, in this study the “1,500-foot” sand and the “1,700-foot” sand are together treated as a single unit.

4. Conclusion

The study finds strong hydraulic connection between the “1,200-foot” sand and the “1,500-foot” sand. Merger of the sand units indicates groundwater recharge from the “1,200-foot” sand to the “1,500-foot” sand. However, there is a distinct clay confining layer to separate the “2,000-foot” sand from the “1,700-foot” sand. The hydrostratigraphy also reveals four sand deposits that compose the “1,500-foot” sand and the “1,700-foot” sand. In general, sand deposition is not uniform, due to spatial and temporal variations in fluvial processes (Chamberlain 2012). The study shows that there is large amount of missing sand in “1,500-foot” sand in the industrial district and in West Baton Rouge Parish, which is possibly due to the presence of an erosional unconformity (Chamberlain 2012).

The sand unit displacement on the Baton Rouge fault and the Denham Springs-Scotlandville fault is significant. The Baton Rouge fault has higher sand displacement than the Denham Springs-Scotlandville fault. Displacement increases over depth. Due to non-uniform fault throw and sand deposition, the study reveals non-uniform flow pathways that connect different sand units at the fault planes. In particular, the identified flow pathways through the Baton Rouge

fault provide important information for understanding patterns of salinization of freshwater aquifers in the East Baton Rouge Parish.

References

- Bense, V.F., and M.A. Person (2006). Faults as conduit-barrier systems to fluid flow in siliciclastic sedimentary aquifers. *Water Resources Research* 42: 18.
- Buono, A. (1983). The Southern Hills regional aquifer system of southeastern Louisiana and southwestern Mississippi. U.S. Geological Survey Water-Resources Investigations Report 83-4189, 38p.
- Chamberlain, E.L. (2012). Depositional environments of upper Miocene through Pleistocene siliciclastic sediments, Baton Rouge aquifer system, Southeastern Louisiana. Louisiana State University, MSc Thesis, 66pp.
- Chilès, J.P., and P. Delfiner (1999). *Geostatistics: modeling spatial uncertainty* Wiley, New York, 734pp.
- Ecology and Environment, Inc. (2011), Recommendations for a statewide ground water management plan (draft), Office of Conservation, Louisiana Department of Natural Resources, DNR Contract No. 2215-10-14, October 21, 2011.
- Elshall, A.S., F.T.-C. Tsai, and J.S. Hanor (2013). Indicator geostatistics for reconstructing Baton Rouge aquifer-fault hydrostratigraphy (Louisiana, USA), *Hydrogeology Journal*. (accepted)
- Griffith, J.M. (2003). Hydrogeologic framework of southeastern Louisiana, Louisiana Department of Transportation and Development Water Resources Technical Report 72 .
- Hansen, N., S.D. Muller, and P. Koumoutsakos (2003). Reducing the time complexity of the derandomized evolution strategy with covariance matrix adaptation (CMA-ES). *Evolutionary Computation* 11: 1-18.
- Hansen, N. (2006). The CMA Evolution Strategy: A Comparing Review. In: Lozano JA, Larrañaga P, Inza I, Bengoetxea E (eds) *Towards a new evolutionary computation, Advances in estimation of distribution algorithms* pp 75-102.
- Hanor, J., E.L. Chamberlain, and F.T.-C. Tsai (2011). Evolution of the Permeability Architecture of the Baton Rouge Fault Zone, Louisiana Gulf Coastal Plain, American Geophysical Union Fall Meeting December 5-9, 2011, San Francisco, CA.
- John, C.J., B.L. Jones, J.E. Moncrief, R. Bourgeois, and B.J. Harder. (1997). An unproven unconventional seven billion barrel oil resource - the Tuscaloosa marine shale, Basin Research Institute Bulletin v7, Louisiana Geological Survey, Baton Rouge, Louisiana.
- Lovelace, J.K. (2009). Groundwater Status in Louisiana, the United States Geological Survey, http://www.epa.gov/region6/water/swp/groundwater/2009-gws-presentations/12-gw-status-in-louisiana_lovelace.pdf, January 5, 2009.
- McCulloh, R.P. and P.V. Heinrich (2012). Surface Faults of the South Louisiana Growth-Fault Province. In: Cox, RT, Tuttle M, Boyd O, Locat J (eds) *Recent Advances in North American Paleoseismology and Neotectonics east of the Rockies and Use of the Data in Risk Assessment and Policy*, Geological Society of America.
- Rollo, J.R. (1969). Salt-water encroachment in aquifers of the Baton Rouge area, Louisiana, Louisiana Department of Conservation, Louisiana Geological Survey, and Louisiana Department of Public Works, pp. 45 p. plus plates.
- Sargent, B.P. (2002). Water use in Louisiana, 2000: Louisiana Department of Transportation and Development Water Resources Special Report no. 15, 133p.

- Sibson, R. (1980). Vector identity for Dirichlet tessellation. *Mathematical Proceedings of the Cambridge Philosophical Society* 87: 151-155.
- Tsai, F.T.-C. (2006). Enhancing random heterogeneity representation by mixing the kriging method with the zonation structure. *Water Resources Research* 42, W08428.
- Tsai, F.T.-C., and W.W.-G. Yeh (2004). Characterization and identification of aquifer heterogeneity with generalized parameterization and Bayesian estimation. *Water Resources Research* 40, W10102.
- Tomaszewski, D. J. (1996). Distribution and movement of saltwater in aquifers in the Baton Rouge area, Louisiana, 1990-1992. Louisiana Department of Transportation and Development Water Resources Technical Report No. 59.
- Welsh, J.H. (2011). Louisiana Commissioner of Conservation Recommendation on Water Sources, dnr.louisiana.gov/assets/OC/2011-TMS-Ground-Water-Resource.pdf, August 2011, Baton Rouge, LA.

6. Student Support

- Ehsan Beigi, doctoral student (starting spring 2011)
- Nima Chitsazan, doctoral student (starting fall 2010)
- Ahmed Elshall, doctoral student (starting fall 2010)

Irregular Wave Dissipation by Coastal Vegetation

Basic Information

Title:	Irregular Wave Dissipation by Coastal Vegetation
Project Number:	2012LA87B
Start Date:	3/1/2012
End Date:	2/28/2012
Funding Source:	104B
Congressional District:	6th
Research Category:	Climate and Hydrologic Processes
Focus Category:	Sediments, Geomorphological Processes, Wetlands
Descriptors:	None
Principal Investigators:	Heather Smith

Publications

There are no publications.

Project Title: Irregular Wave Dissipation by Coastal Vegetation
Start Date: March 1, 2012
End Date: February 28, 2013
Funding Source: 104B
Congressional District: 6
Research Category: Coastal Engineering - Water Resources
Focus Categories: SED, G&G, WL
Keywords: Waves, vegetation, wetlands, turbulence
Principal Investigator: Heather D. Smith

Problem Description

The role of natural coastal defenses in reducing damage from extreme events is a topic of high importance. Events such as the 2004 Indian Ocean Tsunami, Hurricanes Katrina and Rita in 2005, and more recently, Hurricane Sandy in 2012, have continued to illustrate the need for better coastal defenses, and perhaps more importantly, development of accurate predictive models to aid in local evacuation and emergency response planning. Natural coastal defenses include barrier islands, wetlands, and shoals. The sustainability of these regions and therefore their populations and resources, will continue to be an engineering problem for the foreseeable future.

In the planning of coastal restoration projects, wetlands have been identified as desirable due to their buffer capabilities, particularly for reducing storm surge and wave impact. While preliminary data may indicate that the presence of vegetation does reduce wave height, the available data is rather sparse and the actual mechanism for wave reduction is not yet understood. Observations in mangroves by Mazda *et al.* (1997) showed a reduction of wave height from 1.0 m at the front edge of the forest to 0.05 m at the coast for older and denser forests. Newer plantings showed minimal wave reduction. Möller (2006) observed wave attenuation in salt marshes at a variety of depths and wave heights. When the relative wave height (wave height over water depth) became large enough, wave reduction became negligible. Wave attenuation was also small in larger depths where the vegetation was submerged. Wave attenuation was also spatially and seasonally variable, with a dependence on the amount of vegetation cover. Newell and Koch (2004) also observed this dependency of vegetation cover with seagrasses, as no appreciable wave attenuation was observed until the density of the seagrass passed some threshold. The seasonal cycle of the seagrass was also investigated. During the vegetative period, plants are shorter and extend only partially through the water column. This results in a significant decrease in the wave attenuation observed during reproductive periods where the grass extends through most of the water column or is emergent.

A variety of physical experimentation has been performed to investigate fluid-vegetation interactions and estimate the drag coefficient. In studies of emergent vegetation in steady current, Nepf (1999) proposed a cylinder based model where the bulk drag coefficient for the vegetation was calibrated with laboratory data and the influence of plant density and cylinder configuration were examined for Reynolds numbers (UD/ν) of 4,000-10,000. Tanino and Nepf (2008) extended the range of this work by increasing plant density and the range

of the Reynolds number. Of particular interest were Reynolds numbers less than 700, where individual cylinder wake interactions are reduced. The bulk drag coefficient was found to decrease with increasing Reynolds number and solid volume fraction.

In wave environments, Dalrymple *et al.* (1984) proposed a formulation to model the energy dissipation provided by an array of cylinders and the resultant reduction of the wave height. The decay formulation follows

$$K = \frac{H(x)}{H_0} = \frac{1}{1 + \alpha x} \quad (1)$$

where H_0 is the incoming wave height and $H(x)$ is the wave height at location x into the vegetation. The damping factor, α , is given by

$$\alpha = \frac{g^2 C_d N D H_0 (\cosh^2(kl_v) + 2) \sinh(kl_v)}{9\pi k c_g c^3 \cosh^3(kh)} \quad (2)$$

where g is gravity, C_d is the drag coefficient, N is the stem density, D is the stem diameter, k is the wavenumber, l_v is the vegetation height, or the water depth, whichever is smaller, h is the water depth, c_g is the wave group velocity, and c is the group velocity. Several authors (e.g. Augustin *et al.* (2009) and other unpublished works) have utilized this formulation to investigate the relationship of the bulk drag coefficient with other hydrodynamic parameters, including the Reynolds number ($Re = U_w D / \nu$) and Keulegan-Carpenter number ($KC = U_w T / D$) where T is the wave period and U_w is some wave velocity scale often assumed as the maximum velocity. It has been found that the drag coefficient has a higher correlated relationship with Keulegan-Carpenter number.

The wave height decay formulation can also be extended for irregular waves (Mendez and Losada, 2004),

$$K = \frac{H_{rms}(x)}{H_{rms,0}} = \frac{1}{1 + \beta x} \quad (3)$$

where the root-mean-squared (rms) wave heights are utilized. The decay function, β , has a similar form as α in equation (1),

$$\beta = \frac{1}{3\sqrt{\pi}} C_d D N H_{rms,0} \frac{\sinh^3(kl_v) + 3 \sinh(kl_v)}{(\sinh(2kh) + 2kh) \sinh(kh)} \quad (4)$$

In this case, the wavenumber, k , is determined using the peak period, T_p , of the irregular waves.

Methodology

During the summer of 2010, PI Smith and her graduate students participated in a NSF-funded experiment at the O. H. Hinsdale Wave Research Laboratory at Oregon State University. The original study ‘‘Ecological modeling of emergent vegetation for sustaining wetlands in high wave energy coastal environments’’ was proposed by Dr. Daniel Cox and Dr. Denny Ablert at Oregon State University. LSU’s participation was supported by the Louisiana Board of Regents and the Louisiana Water Resources Research Institute. The experiment was performed in the Large Wave Flume, which is 104 m long, 3.7 m wide, and 4.6 m deep.

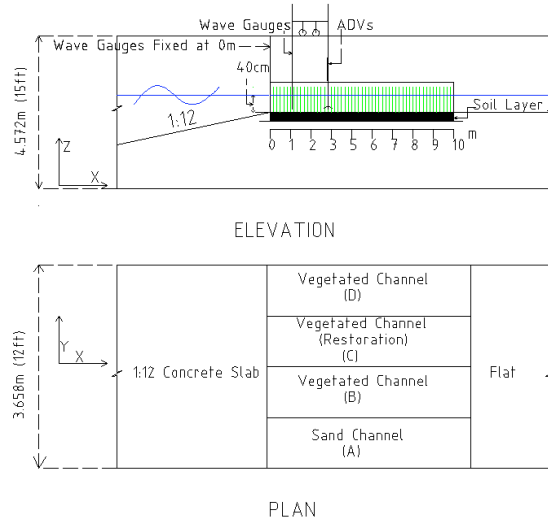


Figure 1: Experimental setup in the Large Wave Flume. Figure is not to scale.

The flume was divided into four, 10 m long channels as shown in Figure 1(a). Three of the four channels were planted with bulrush (*Schoenoplectus pungens*), which is a fairly common species of wetland vegetation growing throughout the United States. Bulrush is a perennial species with the stem having a triangular cross-section for most of the upper part with a circular cross-section at the base. The vegetation used in the experiment were harvested from young natural bulrush beds in the Tillamook Bay of Oregon in the late spring of 2009. The bulrush stems with their root system still intact were cut out in blocks from the inner estuarine regions experiencing low to moderate wave forcing similar to what was simulated in the laboratory. These were then placed in the specially constructed channel boxes and careful preparation was undertaken to sustain their growth throughout the winter of 2009 in the laboratory. The purpose of this exercise was to mimic the field conditions in the best possible way. Channel A was the control sand channel. Channel B had a vegetation density of 1,256 stems/m², Channel C had a vegetation density of 999 stems/m², and channel D had a density of 1,219 stems/m². The majority of the stems in the channel were taller than the location of the free surface. After the initial experiments, the vegetation in channel D was thinned to approximately 630 stems/m².

Wave gauges were placed at the leading edge of each channel and on a moveable platform. This allowed for the observation of the free surface at a variety of locations within the channels. During the three-week experiment, over 200 wave trials were run for the measurement of wave attenuation, and nearly 100 wave trials were run for the investigation of the velocity and turbulence characteristics within the vegetation. The results described here are for wave runs with a 40 cm water depth, leading to fully emergent vegetation. Wave heights of 5-20 cm and wave periods of 1-3 s were considered, which are typically of estuarine waves.

Results

Figure 2 presents the decay curves for the wave height through the vegetated channels. In this figure, the symbols are the laboratory obtained data, while the dashed lines of corresponding color are the best fit curve using Equations (1) for regular waves and (3) for irregular waves. The top panel shows the observations from channel B. The first two runs (blue

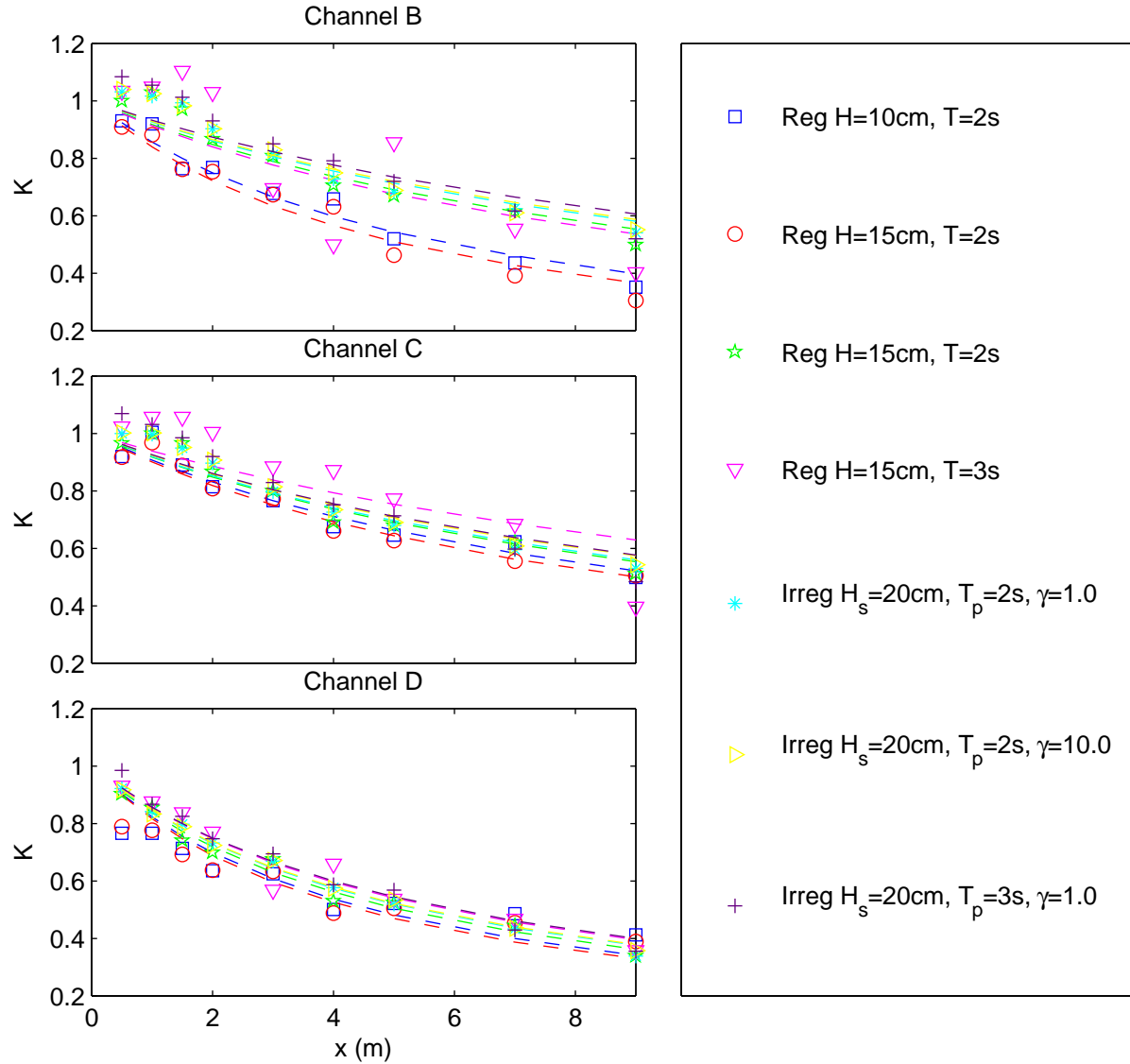


Figure 2: The decay of the wave height $K = H/H_0$ for the vegetated channels for regular and irregular waves. The observations are the symbols and the dashed lines are the best fits using Equations (1) for regular waves and (3) for irregular waves.

squares and red circles) were obtained at the original vegetation density of 1,256 stems/m². The remaining runs were obtained at a roughly 50% lesser density of 630 stems/m². The effect of the different vegetation density is quite marked with a much greater decay with the higher vegetation density. For the remaining panels (Channels C and D), the differences in the two cases for a regular two second wave with an incoming wave height of 15 cm (red circles and green stars) should be similar. In Channels C and D, a small difference in the decay in these two cases is observed. This variation is due to the state of the plant stem. The initial case (red circles) was obtained at the beginning of the experiment, whereas the latter case (green stars) was obtained a week later near the end of the experiment. As the experiment progressed, the stem stiffness reduced due to the combination of repeated wave action and the lack of direct natural light for the plants in the laboratory. The reduced

	α				β		
H_o	10	15	15	15	20	20	20
T	2	2	2	3	2, $\gamma = 1.0$	2, $\gamma = 10.0$	3, $\gamma = 1.0$
γ	N/A	N/A	N/A	N/A	$\gamma = 1.0$	$\gamma = 10.0$	$\gamma = 1.0$
Chan. B	0.168	0.193	0.090	0.096	0.081	0.076	0.072
Chan. C	0.102	0.111	0.090	0.066	0.087	0.083	0.082
Chan. D	0.216	0.226	0.196	0.171	0.185	0.183	0.168

Table 1: Decay coefficients from the best fit lines using Equations (1) for regular waves and (3) for irregular waves.

stem stiffness results in a lesser decay of the waves through the channel. A slight period dependency can be observed, with the smaller period waves decaying more through the vegetation. This is observed for both the regular and irregular wave cases. The effect of the differing wave height is also presented for a 10 cm and 15 cm wave with a period of 2 s. The larger waves show a greater decay in the channel, although the amount of the difference varies from channel to channel.

The irregular wave action can be compared with that of regular waves. The decay for the irregular waves as a given period and is a little larger than for the comparable regular wave case. This may be due to the larger wave height (20 cm) for the irregular waves. Within the irregular waves, the effect of spectral spread parameter ($\gamma = 1.0$ or $\gamma = 10.0$) is small.

Table 1 compares the decay coefficients of the best fit line using Equations (1) for regular waves and (3) for irregular waves. As shown in Figure 2, the effect of the plant density is large. A 50% reduction in plant density (channel B, cases 2 and 3) results in a roughly 50% reduction in the decay coefficient α . This is consistent with Equation (2) in which the stem density N is directly proportional to α . The effect of density and stem height is shown between channels C and D. Channel D had a more consistent and higher stem height than channel C due to the planting nature of the restoration-type planing used in channel C. While the expected reduction in decay values for both α and β due only to different density is around 20%, the decay coefficients actually reduce by around 50%. This is consistent over all of the regular and irregular wave cases.

For irregular waves, the variation of the temporal spectra and wave height distribution across the channel is necessary. Figure 3 presents the 2 s, $\gamma = 1.0$ wave height distribution (top panels) and temporal spectra (bottom panels) across channel D (left to right). Figure 4 presents the 2 s, $\gamma = 10.0$ wave case, and Figure 5 presents the 3 s, $\gamma = 1.0$ wave case. At the beginning of the channel (left panel), the wave height distribution is wide. The blue line is the best fit Rayleigh distribution, which most accurately describes wave height distributions. As the waves progress down the channel, the larger wave heights are reduced. As the number of waves in the channel does not change, this results in a shifting of the distribution toward lower wave heights and a steepening of the distribution. Interesting, the Rayleigh distribution continues to fit the observations reasonably well. The exception to this is the peakier distribution obtained with a spectral spread parameter ($\gamma = 10.0$). In this case, the peak of the distribution is not well described with the Rayleigh distribution. In each panel, the significant wave height, H_s , is presented and represents the average of the highest one-third of the waves.

The influence of the spactral spread parameter, γ , and the change in peak period can be analyzed with the bottom panels of the Figures. A spectral spread parameter of $\gamma = 1.0$ results in a wider spectra that is more consistent with locally generated waves in estuarine environments. The greater spectral spread parameter of $\gamma = 10.0$ results in a sharper spectra more consistent with offshore generated storm waves. The highest peak in the spectra is the location of the peak period, T_p . The location of the peak period does not change significantly between locations within the channel. The total energy within the spectra does decrease with distance into the channel. This results in a majority of the remaining spectral energy consilodating around the peak period. As a result of the consilodation of the wave energy around the peak period and the steepening of the wave height distribution, the waves are becoming more regular as they progress through the vegetation.

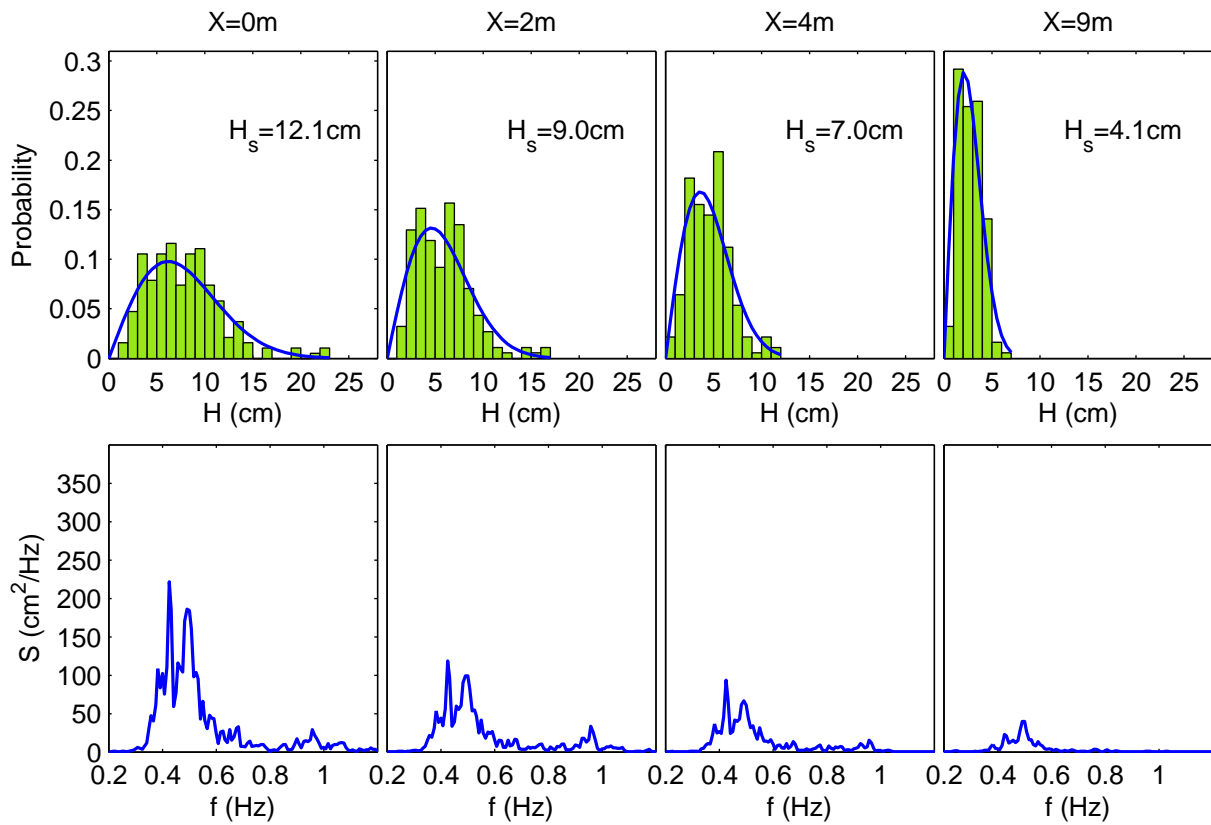


Figure 3: The wave height distribution (top panels) and temporal spectra (bottom panel) for the 2 s, 20 cm wave case with a spectral spread parameter of $\gamma = 1.0$.

Conclusions

Wetland vegetation is potentially significant solution to help mitigate storm generated waves along the coastline. As shown in this research, wave attenuation of upwards of 60% were observed within the first 10 m of a vegetated channel. The dependency of the amount of wave attenuation on a variety of wave and vegetation characteristics are tested with live vegetation in a controlled laboratory environment. As predicted by theory, the amount of damping is dependent on the density of the vegetation. A reduction of the vegetation density

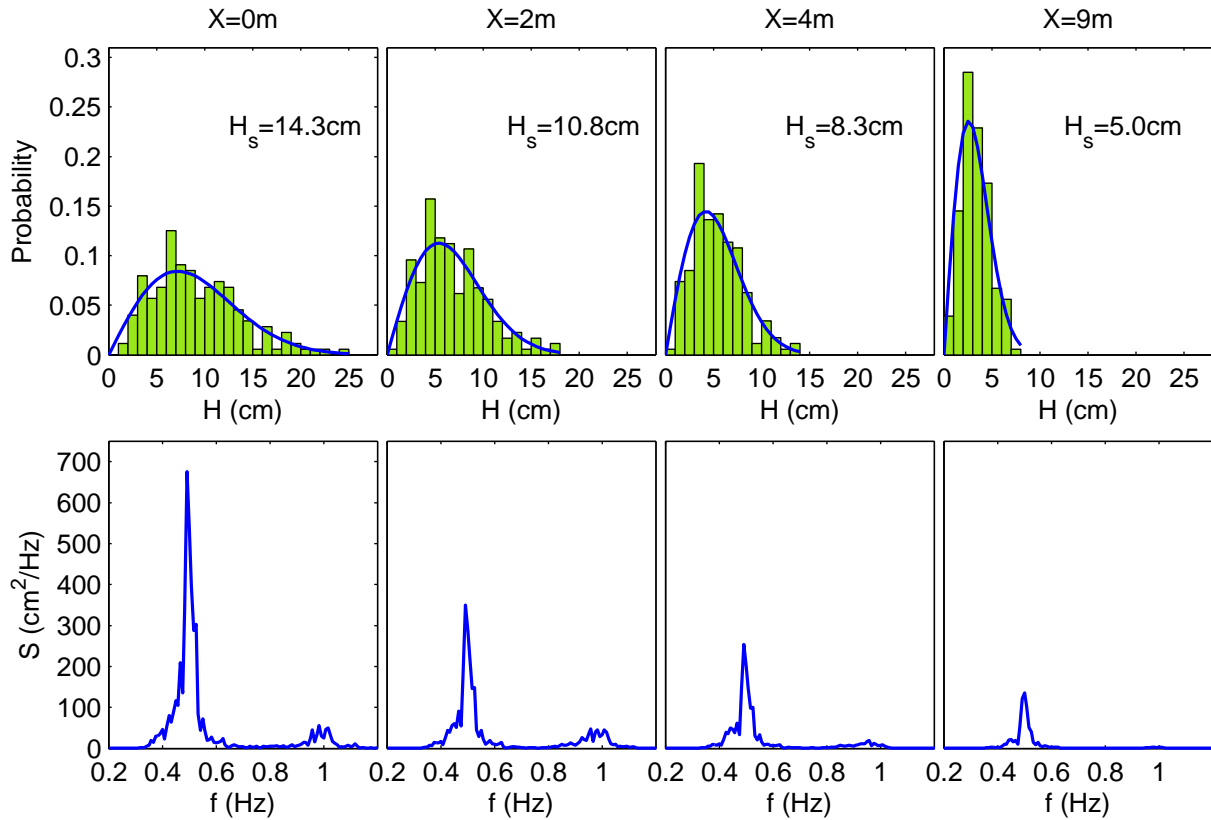


Figure 4: The wave height distribution (top panels) and temporal spectra (bottom panel) for the 2 s, 20 cm wave case with a spectral spread parameter of $\gamma = 10.0$.

of 50% resulted in a reduction in the dampening capability of the vegetation by 50% as well. Additionally, the stiffness of the plant itself can also be a contributing factory to the amount of dissipation provided. However, the mechanism for including these factors is imperfect and is lumped into the drag coefficient, C_d . This presents a difficulty for researchers utilizing these theoretical models, as the same vegetation patch may have a different performance depending on these hard to quantify plant characteristics. The consistency of the height of the vegetation was also shown to have an effect. Consistently higher stems produced more dissipation than those with a greater stem variability, like newly planted restoration wetlands.

In terms of wave characteristics, lower wave periods were shown to be more susceptible to damping. Waves with a greater wave height were shown to decay more through the vegetation. In our study irregular waves showed slightly greater decay than a similarly sized regular wave field. However, it is unclear if this increased decay is due to the irregular nature of the waves, or to the wave height for the irregular waves being 5 cm larger. Irregular waves were found to continue to fit the Rayleigh distribution reasonably well throughout the vegetation. The exception to this was the wave case with a well defined and sharp spectrum. In this case, the Rayleigh distribution does not match as well at any point, including the incoming wave field at the upstream edge of the vegetation. Due to the preferential damping of the larger waves, the wave heights are reduced and tend move towards a regular wave

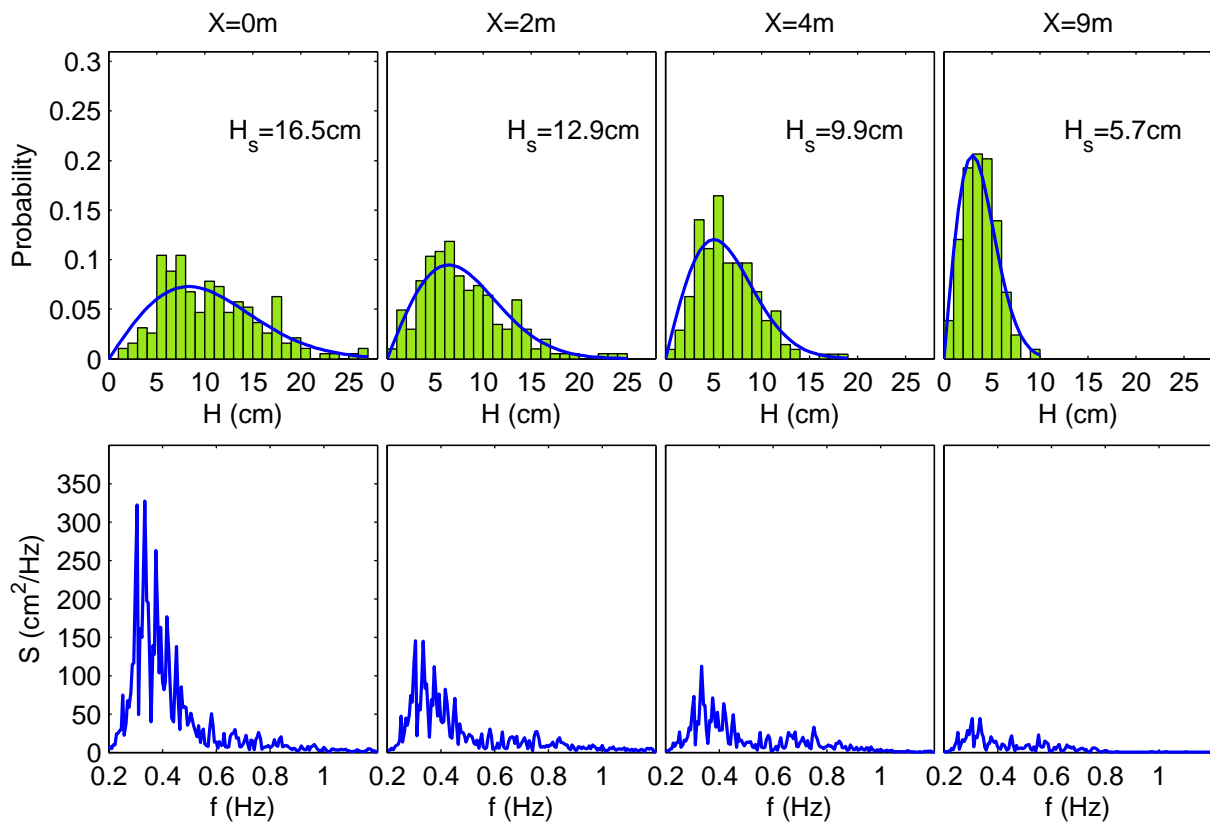


Figure 5: The wave height distribution (top panels) and temporal spectra (bottom panel) for the 3 s, 20 cm wave case with a spectral spread parameter of $\gamma = 1.0$.

field. The peak period did not show any significant changes through the vegetation.

References

- Augustin, L. N., Irish, J. L., and Lynett, P. (2009). Laboratory and numerical studies of wave damping by emergent and near-emergent vegetation. *Coast. Eng.*, 56(3):332–340.
- Dalrymple, R. A., Kirby, J. T., and Hwang, P. A. (1984). Wave diffraction due to areas of energy dissipation. *J. Waterw., Port, Coastal, Ocean Eng., ASCE*, 110(1):67–79.
- Mazda, Y., Magi, M., Kogo, M., and Hong, P. N. (1997). Mangroves as a coastal protection from waves in the Tong King delta, Vietnam. *Mangroves and Salt Marshes*, 1(2):127–135.
- Mendez, F. J. and Losada, I. J. (2004). An empirical model to estimate the propagation of random breaking and nonbreaking waves over vegetation fields. *Coast. Eng.*, 51(2):103–118.
- Möller, I. (2006). Quantifying saltmarsh vegetation and its effect on wave height dissipation: Results from a UK East coast saltmarsh. *Est. Coast. Shelf Sci.*, 69(3-4):337–351.
- Nepf, H. M. (1999). Drag, turbulence, and diffusion in flow through emergent vegetation. *Water Resour. Res.*, 35(2):479–489.

- Newell, R. I. E. and Koch, E. W. (2004). Modeling seagrass density and distribution in response to changes in turbidity stemming from bivalve filtration and seagrass sediment stabilization. *Estuaries*, 27(5):793–806.
- Tanino, Y. and Nepf, H. M. (2008). Laboratory investigation of mean drag in a random array of rigid, emergent cylinders. *J. Hydraul. Eng., ASCE*, 134(1):34–41.

Information Transfer Program Introduction

Because of the Deep Horizon oil spill, our efforts for information transfer were dominated by that activity again in FY 2012. Full details are provided in the “Notable Achievements” section of the report. Highlights of our activities are listed below:

- LWRRI built and managed a collaborative web review process for the Deep Water Horizon Science and Engineering Review Team immediately after the spill. This allowed for rapid review of dozens of documents and storage of GB's of information for review by statewide academic members of the team. This activity continued into FY 2012.
- LWRRI participated in organizing scientific conferences and symposia related to DH Spill (Chaired session at LSU DWH Conference in early Spring 2013; presented papers at GOMRI conference in New Orleans in 2012)
- LWRRI is coordinating research and damage assessment for the Wisner Donation property in Lafourche Parish, one of the 10 largest landowners in the state. The Wisner Donation property includes 35,000 acres including Fourchon Beach. Through this activity, LWRRI participated in several meetings with Gulf Coast Incident Management Team (official clean-up personnel with Coast Guard, USGS, BP and others).
- LWRRI is working with Point au Chiene tribe in understanding impacts from DH spill on marshes in Barataria Basin, LA.
- LWRRI was the chief sponsor of the LSU Environmental Film Series in March and April 2012 at LSU. The following films included: Revenge of the Electric Car and One Water. These films were followed by discussions with students and faculty organized by LWRRI. Attendance averaged 120 per night.

USGS Summer Intern Program

None.

Student Support					
Category	Section 104 Base Grant	Section 104 NCGP Award	NIWR-USGS Internship	Supplemental Awards	Total
Undergraduate	5	0	0	0	5
Masters	2	1	0	0	3
Ph.D.	8	3	0	0	11
Post-Doc.	0	0	0	0	0
Total	15	4	0	0	19

Notable Awards and Achievements

Of note in FY2012 was LWRRI's participation in response to the Deepwater Horizon Oil Spill, the largest spill in US history. Details are presented below.

LWRRI advised response agencies

- Advised the state through the Horizon Science and Engineering Review Team (H-SERT), a group of academic experts who worked with state trustees on the response. LWRRI Director Pardue led one of the standing committees in H-SERT and participated by reviewing and commenting on dozens of documents and plans. LWRRI set up a collaborative web review process for H-SERT which allowed participating by academics across the state. Pardue also participated in helicopter tours with the lead trustee agency, the Office of Coastal Protection and Restoration.
- Dr. Pardue has also provided comments on many plans and remediation strategies ongoing through 2013
- Service on national American Petroleum Institute committee on "Use of Dispersants in the Deep Ocean"

LWRRI Conducted Research on the Spill

- LWRRI Director Pardue is coordinating research and damage assessment for the Wisner Donation property in Lafourche Parish, one of the 10 largest landowners in the state. The Wisner Donation property includes 35,000 acres including Fourchon Beach. Dr. Pardue has travelled to Wisner areas to conduct research an average of once per week since October 2010.
- Received research funding from LSU GOMRI BP fund and Wisner Donation
- Fifteen students (undergraduate, MS and PhD) have been involved in this activity to date.

LWRRI organized conferences and presented research results

- Organizing scientific conferences and symposia related to DH Spill (Steering committee of DWH conference at LSU in 2013; presentations at GOMRI conference in New Orleans in 2012
- Numerous media appearances regarding oil spill recovery including long interview on NPR Marketplace through the show BURN, an energy journal, April 2012

Publications from Prior Years